Development of a Multiprocessing Performance Test System of Multi-Pixel Photon Counters for Super-Fined Grained Detector

(Super-FGD検出器用MPPCのマルチプロセス性能試験システムの開発)

Yoshimi Yoshimoto

Department of Physics, University of Tokyo

December 7, 2021

Abstract

T2K is a long baseline neutrino oscillation experiment measuring θ_{23}, θ_{13} and Δm_{23}^2 from observation of muon neutrino disappearance and electron neutrino appearance, from which CP violation in lepton sector can be studied. T2K collaboration is planning to upgrade near detector to better constrain neutrino interaction systematics.

Super-Fine Grained Detector (SuperFGD) will be a new detector in the upgraded detector. SuperFGD utilizes 56,384 multi-pixel photon counters (MPPC), thus it is important to understand their behaviour before installation. A performance test system for those MPPC-PCBs (printed circuit boards) is under development. The test system aims to measure and analyze their dark noise, gain, photon detection efficiency, cross talk and operation voltage.

This thesis discusses the development of parallel test setups in the test system and their systematic performance, as well as measurement results of the first batch of MPPC-PCBs.

Contents

Chapter 1

Introduction

1.1 Neutrino oscillation and *CP* violation

The Standard Model is a fundamental theory of particle physics that describes how elementary particles interact under three fundamental forces. While bringing out huge successes in experimental predictions, the Standard Model is mostly self-consistent but not complete, as it leaves some phenomena unexplained [1].

In the framework of the Standard Model, neutrinos are described as massless particles that come in three different flavours, electron neutrinos (ν_e), muon neutrinos (ν_μ), and tau neutrinos (ν_τ). Each flavour is associated with a corresponding antiparticle. However, several breakthroughs in neutrino physics indicate that neutrinos have three mass eigenstates that are not identical to flavour eigenstates. It is experimentally observed that neutrinos change from one flavour to another during their propagation, which indicates that neutrinos are massive. This phenomenon is called neutrino oscillation and was elaborated by Bruno Pontecorvo [2] [3], Maki, Nakagawa, and Sakata [4] in the 1960s. Pontecorvo–Maki–Nakagawa–Sakata matrix (PMNS matrix) describes the mixing of the eigenstates as:

$$|\nu_i\rangle = \sum_\alpha U_{\alpha i} |\nu_\alpha\rangle , \qquad (1.1)$$

$$|\nu_\alpha\rangle = \sum_i U_{\alpha i}^* |\nu_i\rangle , \qquad (1.2)$$

where:
$|\nu_\alpha\rangle$ is a neutrino with definite flavor α = e (electron), μ (muon) or τ (tauon),
$|\nu_i\rangle$ is a neutrino with definite mass m_i with i=1,2,3,
$U_{\alpha i}$ represents the PMNS matrix, and $U_{\alpha i}^*$ is its complex conjugate.

The ultrarelativistic limit, $|\vec{p_i}| = p_i \gg m_i$, can be applied in calculation since all currently observed practical neutrinos have mass ($<$1 eV) farther less than their energy ($>$1 MeV). Under this limit, the probability that a neutrino

with energy E of flavour α oscillate to flavour β after traveling a certain distance L can be calculated as [5]:

$$P_{\nu_\alpha \to \nu_\beta}(L, E) = |\sum_i U_{\alpha i}^* U_{\beta i} e^{-i\frac{m_i^2 L}{2E}}|^2 \tag{1.3}$$

$$= \delta_{\alpha\beta} - 4\sum_{i>j} \mathfrak{Re}(U_{\alpha i}^* U_{\beta i} U_{\alpha j} U_{\beta j}^*) \sin^2(\Delta m_{ij}^2 \frac{L}{4E}) \tag{1.4}$$

$$+2\sum_{i>j} \mathfrak{Im}(U_{\alpha i}^* U_{\beta i} U_{\alpha j} U_{\beta j}^*) \sin(\Delta m_{ij}^2 \frac{L}{2E}), \tag{1.5}$$

where

$$\Delta m_{ij}^2 = m_i^2 - m_j^2 \tag{1.6}$$

is the squared mass difference of neutrinos. Anti-neutrinos have the same kinematical properties as neutrinos, while the mixing matrix should be its complex conjugation. Thus, the anti-neutrino oscillation probability can be written as:

$$P_{\bar{\nu}_\alpha \to \bar{\nu}_\beta}(L, E) = |\sum_i U_{\alpha i}^* U_{\beta i} e^{-i\frac{m_i^2 L}{2E}}|^2 \tag{1.7}$$

$$= \delta_{\alpha\beta} - 4\sum_{i>j} \mathfrak{Re}(U_{\alpha i}^* U_{\beta i} U_{\alpha j} U_{\beta j}^*) \sin^2(\Delta m_{ij}^2 \frac{L}{4E})$$

$$-2\sum_{i>j} \mathfrak{Im}(U_{\alpha i}^* U_{\beta i} U_{\alpha j} U_{\beta j}^*) \sin(\Delta m_{ij}^2 \frac{L}{2E}). \tag{1.8}$$

The PMNS matrix is a square matrix of rank three when the standard three-neutrino theory is considered, but can be larger when more generations are added. In the three generation case, the PMNS matrix can be parameterized by three mixing angles (θ_{12}, θ_{23}, θ_{13}) and one complex phase δ_{CP} [6]:

$$U = \begin{bmatrix} U_{e1} & U_{e2} & U_{e3} \\ U_{\mu 1} & U_{\mu 2} & U_{\mu 3} \\ U_{\tau 1} & U_{\tau 2} & U_{\tau 3} \end{bmatrix}$$

$$= \begin{bmatrix} 1 & 0 & 0 \\ 0 & c_{23} & s_{23} \\ 0 & -s_{23} & c_{23} \end{bmatrix}_{(a)} \begin{bmatrix} c_{13} & 0 & s_{13}e^{-i\delta_{CP}} \\ 0 & 1 & 0 \\ s_{13}e^{i\delta_{CP}} & 0 & c_{13} \end{bmatrix}_{(b)} \begin{bmatrix} c_{12} & s_{12} & 0 \\ -s_{12} & c_{12} & 0 \\ 0 & 0 & 1 \end{bmatrix}_{(c)} \tag{1.9}$$

$$= \begin{bmatrix} c_{12}c_{13} & s_{12}c_{13} & s_{13}e^{-i\delta_{CP}} \\ -s_{12}c_{23} - c_{12}s_{23}s_{13}e^{-\delta_{CP}} & c_{12}c_{23} - s_{12}s_{23}s_{13}e^{i\delta_{CP}} & s_{23}c_{13} \\ s_{12}s_{23} - c_{12}c_{23}s_{13}e^{-i\delta_{CP}} & c_{12}s_{23} - s_{12}c_{23}s_{13}e^{i\delta_{CP}} & c_{23}c_{13} \end{bmatrix},$$

where s_{ij} and c_{ij} are $\sin\theta_{ij}$ and $\cos\theta_{ij}$ respectively. The compex phase δ_{CP} is related to charge-parity (CP) violations. The CP violation is a combined

particle-antiparticle asymmetry of charge conjugation (C) and spatial symmetry (parity P). The existence of CP violation is crucial to the plausible explanation of why matter dominates the universe, but almost no anti-matter exists. The Standard Model allows CP violation in weak interaction by adding the complex phase δ_{CP} to the PMNS matrix as shown in Equation 1.9. In Equation 1.5, the oscillation probability of particle and anti-particle differs only in the imaginary part. The difference can be expressed as [7]:

$$A_{\alpha\beta}^{CP}(L, E) = 4 \sum_{i>j} \mathfrak{Im}(U_{\alpha i}^* U_{\beta i} U_{\alpha j} U_{\beta j}^*) \sin(\Delta m_{ij}^2 \frac{L}{2E}), \qquad (1.10)$$

suggesting that the CP term can be only measured when $\alpha \neq \beta$. Looking for CP violation in the lepton sector is very important because that in the strong sector and quark sector is measured to be not sufficient for explaining the matter-antimatter imbalance in our Universe [8].

As discussed, neutrino oscillation opens a window for determining the CP violation term in the lepton sector, which requires precise measurements of matrix parameters. Many experiments are done or ongoing in order to measure those parameters. In Equation 1.9, the PMNS matrix is factorized into three parts. The atmospheric term (a) can be determined by atmospheric and long-baseline accelerator neutrino experiments. The mixed term (b) can be determined by long-baseline accelerator experiments and short-baseline reactor experiments. The solar term (c) can be determined by solar and long-baseline reactor experiments [9]. After all, long-baseline experiments played an important role in confirming neutrino oscillation and measuring parameters. Fixed baselines and detectors provide good energy resolutions, enabling precise measurements of L/E for individual events.

1.1.1 Neutrino mass ordering

Current oscillation data is sensitive to neutrino mass in terms of two squared mass differences. Δm_{21}^2 is known to be positive due to the matter effects in the sun. However, the sign of atmospheric mass splitting Δm_{31}^2 is currently undetermined because it is measured only via neutrino oscillations in vacuum. Thus, there are two possible neutrino mass ordering: $\Delta m_{31}^2 > 0$ as *normal* and $\Delta m_{31}^2 < 0$ as *inverted*[10].

1.2 Neutrino interaction

Neutrino interactions are described by the Standard Model without any deviation discovered so far. Neutrino experiments are detecting products of neutrino interaction because neutrinos cannot be directly detected due to their electrical neutrality. Thus, understanding neutrino interactions with matter is essential in neutrino oscillation measurements. The Charged-Current Quasi-Elastic (CCQE) is a two-body interaction that dominates the low energy ($<$
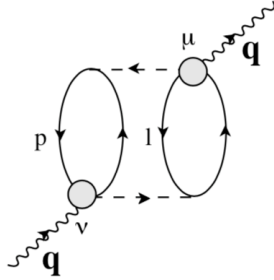
Figure 1.1: Two particle−two hole W − selfenergy Feynman diagram where the outgoing gauge boson couples to the second nucleon [14]

1 GeV) CC process in the accelerator-based long-baseline neutrino oscillation experiments:

$$\nu_l + n \rightarrow \ell + p, \tag{1.11}$$

$$\bar{\nu}_l + p \rightarrow \bar{\ell} + p. \tag{1.12}$$

Well-measured kinematics of the final state of lepton kinematics can provide the initial neutrino energy without the reconstruction of final hadronic energy for CCQE [11]. CCQE is the dominant interaction for the neutrino energy between 0.3 GeV to 3 GeV.

Two-particle-two-hole (2p2h) excitation is also an important multi-nucleon interaction effect in neutrino-nucleus interactions modelling. It has no pions in the final state, as shown in Figure 1.1, so 2p2h events can be misidentified as QE events, which also have no pions in the final states [12]. It can be problematic because neutrino oscillation experiments employ QES (CCQE) to assign neutrino energies. 2p2h components misidentified as QE events will pick up a bias which is typically 100 MeV below the true neutrino energy [13]. Generally, low momentum protons can be used as clues to distinguish 2p2h events from QE events.

1.3   T2K experiment

T2K("Tokai to Kamioka") experiment is a long-baseline neutrino oscillation experiment physically based in Japan. T2K uses the off-axis neutrino beam from Japan Proton Accelerator Research Complex(J-PARC) and takes measurements by both near detectors and Super-Kamiokande as the far detector. Figure 1.2 is an overview of the T2K experiment.
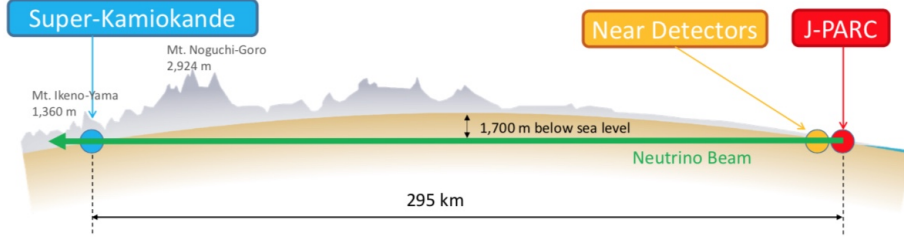
Figure 1.2: T2K Overview [15]

T2K experiment measures θ_{23}, θ_{13} and Δm_{23}^2 from observation of muon neutrino disappearance and electron neutrino appearance. In a simple case, the oscillation probability of muon neutrino oscillate to electron neutrino can be approximated as following in the vacuum [16]:

$$P(\nu_\mu \to \nu_e) \simeq \underbrace{4|\mathcal{T}_3^{\mu e}|^2 \sin^2 \Delta_{31}}_{\text{atmospheric}} + \underbrace{4|\mathcal{T}_2^{\mu e}|^2 \sin^2 \Delta_{21}}_{\text{solar}}$$
$$+ \underbrace{8|\mathcal{T}_2^{\mu e}||\mathcal{T}_3^{\mu e}| \sin \Delta_{31} \sin \Delta_{21} \cos(\Delta_{32} + \delta)}_{\text{interface}}, \quad (1.13)$$

where

$$\Delta_{ji} = \Delta m_{ji}^2 L / 4E, \quad (1.14)$$

$$\mathcal{T}_3^{\mu e} = \frac{1}{2} \sin 2\theta_{13} \sin \theta_{23} e^{i\delta_{CP}}, \quad (1.15)$$

$$\mathcal{T}_2^{\mu e} \simeq \frac{1}{2} \sin 2\theta_{12} \cos \theta_{13} cos \theta_{23}. \quad (1.16)$$

While solar term $\sin^2 \Delta_{21}$ is small at T2K's L/E, the resulting oscillation mainly comes from atmospheric term and interface term. The CP-independent atmospheric term provides five times the amplitude than the interface term and thus dominates oscillating results. It is still possible to bring up direct measurement of phase CP from the interface term [16]. In Equation 1.13, the CP violation term $\sin \delta_{CP}$ takes a negative sign for neutrinos and a positive sign for anti-neutrinos, so the CP phase can be fitted from the difference of neutrino and anti-neutrino appearance probability. For T2K, the matter effect dominates the solar term when added into the calculation but provides relatively small perturbations to atmospheric and interface term. This perturbation effect gives T2K some sensitivity to neutrino mass ordering.

1.3.1 T2K neutrino beam

T2K experiment uses the muon neutrino beam produced in J-PARC. Primary proton beam is accelerated by J-PARC main ring accelerator then hits on
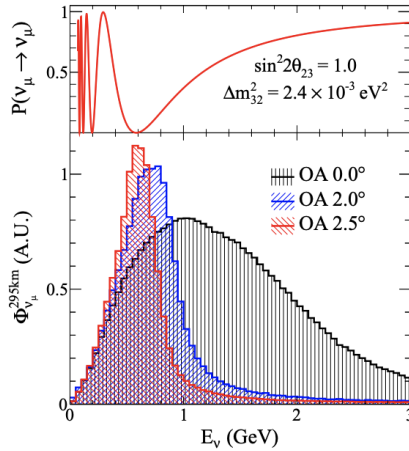
Figure 1.3: Muon neutrino survival probability at 295 km and neutrino fluxes for different off-axis angles [17]

graphite target and generates secondary hadrons. Those hadrons, mainly pions and kaons, are focused and selected by the sign of charge in three electromagnetic horns. Those horns operate at a current of +250 kA in ν mode or -250 kA for $\bar{\nu}$ mode. Then the selected ones travel to a decay volume and decay through the reaction:

$$\pi^{\pm} \rightarrow \mu^{\pm} + \overset{(-)}{\nu}_{\mu}. \tag{1.17}$$

Finally, a beam dump stops remaining protons and hadrons, and the resulting beam goes through the muon monitor (MUMON), which detects muon above 5 GeV and checks the beam stability.

As mentioned, T2K uses the off-axis beam technique to narrow the peak at about 0.6 GeV in the neutrino energy spectrum at the far detector (SK) [17]. The angle is tuned to be 2.5°so that SK can have an expected oscillation maximum. The prediction of the neutrino flux at the far detector is shown in Figure 1.3 [16].

A typical main ring beam power during T2K operation in March 2021 is 510 kW. J-PARC main ring accelerator will shut down for one year in 2021 to upgrade beam power and should reach 750 kW in 2022 [18].

1.3.2 Near Detector Complex

T2K near detector complex locates nearly 280 meters away from the production target. It directly measures neutrino property and neutrino interaction rate before oscillation and allows a prediction of the expected spectra at the far de-

tector to reduce model-based uncertainties in analysis for precise measurement [19].

INGRID

INGRID is an on-axis detector designed to be a separate array of iron/scintillator and measures the neutrino beam direction and profile. Figure 1.4 shows the structure of the INGRID module.
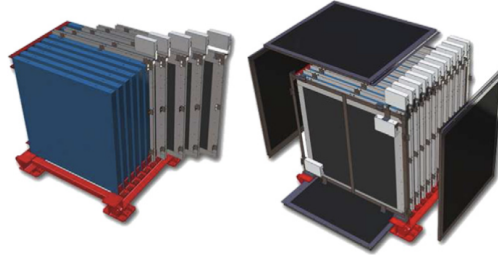
Figure 1.4: A INGRID module [20]

ND280 Complex

ND280 is an off-axis detector placed at the same azimuthal angle as the direction of Super-Kamiokande to mitigate the directional effect. It measures flux and properties of neutrino interactions and constrain the neutrino interaction systematic. ND280 is also designed to be immersed in a magnetic field, enabling the detection and identification of leptons and measures intrinsic electron neutrino contamination in the beam. The T2K collaboration is planning to upgrade ND280 to reduce systematic uncertainty, which is discussed in Section 1.4.

WAGASCI-Baby MIND

WAGASCI-Baby MIND is a new detector devoted to neutrino interaction studies, located next to the INGRID and ND280 detectors [21].

1.3.3 Far Detector

T2K uses Super-Kamiokande (SK), a large underground water Cherenkov detector 295 km away from J-PARC, as the far detector. SK uses water as the target and introduces gadolinium to improve detection ability. The wall of the water tank is covered by 20-inch photo-multiplier tubes (PMTs), which are very sensitive to Cherenkov photons from the leptons generated in neutrino interactions. Figure 1.5 shows the inner look of the SK water tank and PMTs used in SK [22].

<center>(a)   (b)</center>
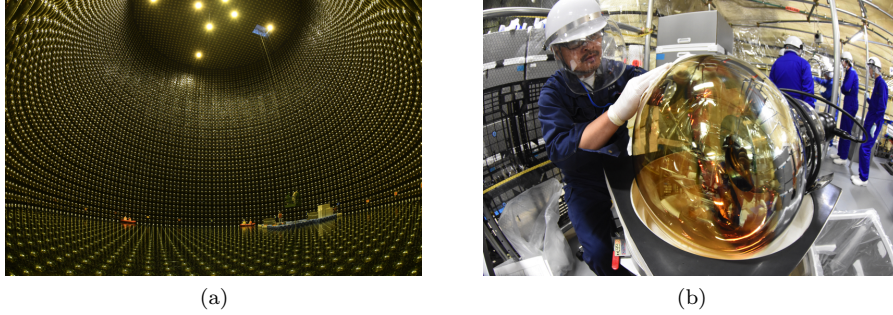
Figure 1.5: (a):Inner look of the SK Water Tank;(b) SK PMTs under inspection and covering

1.3.4 Latest results of T2K

By May/10/2021, T2K has analyzed the data set collected from an exposure of $14.9(16.4) \times 10^{20}$ protons on target in (anti)neutrino mode, collected between 2010 and 2018. Assuming normal mass ordering, T2K reports $\sin^2 \theta_{23} = 0.53^{+0.03}_{-0.04}$ and $\Delta m^2_{32} = (2.45 \pm 0.07) \times 10^{-3} eV^2 c^{-4}$, and also excludes CP conservation in neutrino oscillation at the 2σ level. T2K has disfavoured half of the possible values of the CP violation phase in the lepton sector at the confidence level of $99.7\%(3\sigma)$. In the future, T2K will collect more data and include more complex event topologies in the analyses. Future joint analyses with SK and NOνA, the NuMI Off-axis ν_e Appearance experiment at Fermilab, are also planned. Detailed information can be found in [16].

1.4 ND280 upgrade

1.4.1 Current ND280 and its weakness

ND280 is very important in understanding the neutrino beam sent to SK, as discussed in Section 1.3.2. It is designed to have the capacity of reconstructing exclusive neutrino CCQE, CC inelastic, neutral current events and measuring inclusive events rate [20]. Current ND280 consists of several components as shown in Figure 1.6. The P∅D(pi-zero detector) is located upstream inside the metal frame, followed by the TPC (time projection chamber)/FGD (fine-grained detector) sandwich. The metal container is called a "basket" and surrounded by Ecal (electromagnetic calorimeters). ND280 utilizes the recycled UA1 magnet to provide the 0.2T magnetic field and instrumented with scintillator planes as the SMRD (side muon range detector). Specifically, those detectors serve different purposes.

P∅D measures the neutral current process on a water target. TPC measures the number, direction, momentum and ionization of traversing and generated charged particles in detectors, providing some degrees of particle identification.

<center>11</center>
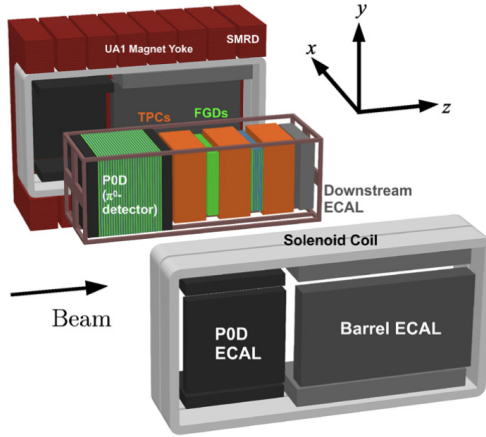
Figure 1.6: ND280 Detector [20]

FGDs serves both as target mass and a particle tracking detector. Ecals function to measure photon energy and direction and collect information of charged particles for identification. Finally, SMRD records muons escaping with high angles and cosmic-ray muons that enter or penetrate the ND280 detector.

In general, ND280 is very powerful in selecting clean samples of muon neutrinos and muon anti-neutrinos. The main strength of the ND280 is that its magnetization allows the determination of lepton charge and momentum produced by neutrino interactions. Moreover, ND280 can perform particle identification, particularly between muons and electrons, because of TPCs and Ecals. ND280 data has been used for all the T2K oscillation analyses and reduced uncertainties due to neutrino fluxes and cross-sections from aboout 15% to 6% uncertainties [23]. Powerful as it is, the current ND280 still leaves some weakness to be improved.

The main limitation of the current ND280 is that the detection efficiency drops significantly when the scattering angles is larger than about 40 degrees with respect to the beam direction because of the vertical arrangement and sandwiched structure of TPC and FGD, as shown in Figure 1.7. In contrast, Super-Kamiokande provides a full angle detection with respect to the beam direction. Thus, improvements in the near detector sensitive angle should be considered. Moreover, short tracks that end in FGD can only be seen in two dimensions so that the tracking efficiency is bad at low momentum, especially for protons. Figure 1.8 shows the reconstruction efficiency in the ND280. Another weakness is that it does poorly in selecting electron neutrino interactions below 1 GeV. This low efficiency, coming with the large photon background, limits T2K's ability on electron neutrino cross-section measurement [23].
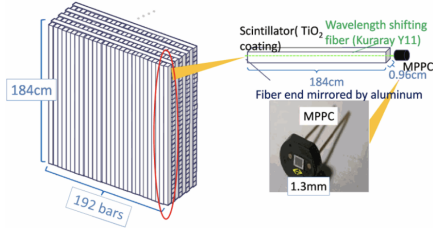
Figure 1.7: FGD structure [24]
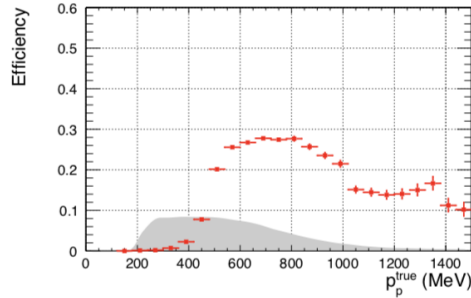
Figure 1.8: Proton reconstruction efficiency in ND280. The grey histogram corresponds to spectrum of generated protons accting to NEUT MC [25]

1.4.2 Design of upgraded ND280

In general, the goal of ND280 upgrade is to lower the ND280-led systematic errors, currently of the order of 6%, to about 4% for T2K-II and to about 3% for Hyper-Kamiokande. In order to improve the performance of ND280, T2K is planning to add a new highly granular 3D scintillator detector SuperFGD and two high-angle atmospheric pressure TPCs (HA-TPC) in the upstream direction of the current TPC/FGD array. These detectors are surrounded by six large TOF (time-of-flight) planes to determine the track direction and improve particle identification. Figure 1.9 gives a designed configuration of the upgrade detector. This new configuration provides more targets and enables the full polar angle acceptance for muons produced in neutrino interactions[25].

SuperFGD

As both target and detector to reconstruct near-vertex tracks, scintillator detectors should be massive enough to provide enough target, as well as able to accept charge lepton and reconstruct short tracks of low energy hadrons. Figure 1.10 shows a schematic concept of the SuperFGD structure. SuperFGD
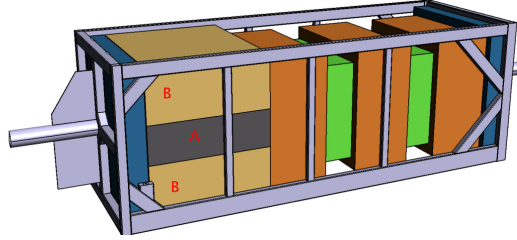
Figure 1.9: Upgrade ND280 detector. SuperFGD is labelled as A. High-Angle TPCs are labelled as B.[23]
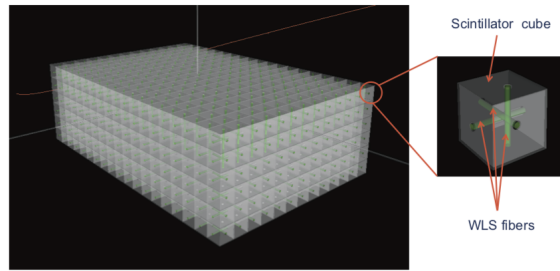
Figure 1.10: Schematic concept of SuperFGD structure.[25]

consists of $192 \times 184 \times 56$ optically independent 1cm^3 plastic scintillator cubes.

Wavelength shifting(WLS) fibers run through the volume to read out light signals generated in the volume can be along three orthogonal directions. Figure 1.11 shows the direction of the signal flow designed in SuperFGD.

Multi-Pixel Photon Counters(MPPC) will be used for scintillation light detection, instrumented at ends of WLS fibers. They will be placed on the upstream, top, left and right side of the detector. Fronted electronics will be placed on the left and right sides of the detector.

With these designs, the SuperFGD can detect signals along three axis and thus enables 3D reconstruction.

High-Angle TPC

TPCs in the current ND280 has been proved to be very useful. Thus, upgraded High-Angle TPCs is designed to perform substantially similar to existing TPCs. The main structure of TPC is a TPC field cage which provides a highly uniform electrostatic field containing high-purity mixed gas as shown in Figure 1.12. Charges generated from the ionization of gas will be drifted along the magnetic field direction towards the readout anodes. Similar to the existing

14
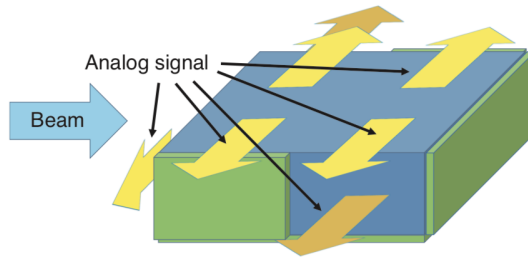
Figure 1.11: SuperFGD signal flow.[25]
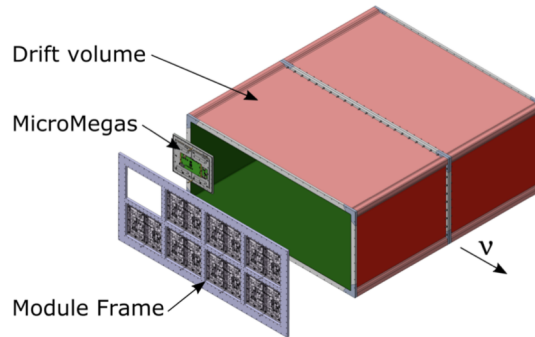
Figure 1.12: Schematic concept of HA-TPC.[25]

TPC, HA-TPC will enable charge and momentum measurement and 3D track reconstruction. When combined with energy deposit measurement, HA-TPC is also possible to perform particle identification.

TOF

Time of fight detector is a full closure for SuperFGD and HA-TPCs, as shown in Figure 1.13, aiming to precisely measure the crossing time of charged particles in ND280. TOF can distinguish the neutrino interaction in the target from backgrounds originating events, and help particle identification.

1.5 Expectation of upgrade detectors

In general, because the ND280 upgrade detector is under construction, the performance of the ND280 Upgrade detector is evaluated from data rendered simulations. The detector geometry and particle trajectory in the detector are simulated by GEANT4. The neutrino beam prediction is obtained by

Figure 1.13: Schematic concept of TOF.[25]

JNUBEAM simulation for both neutrino mode and anti-neutrino mode [23].

1.5.1 SuperFGD detector response

The track reconstruction efficiency in the SuperFGD has been studied for pion, proton and muon. Figure 1.14 shows the reconstruction efficiency for muons, pions and protons as a function of momentum and angle of the particle track with respect to the beam direction, demonstrating both calculations down by three-dimensional information and two-dimensional information. The benefit of the three-dimensional reconstruction is quite apparent.

Compared to FGD, SuperFGD can reconstruct particle tracks with higher efficiencies for all angles and have a lower momentum threshold. The left plot in Figure 1.15 demonstrates the reconstruction efficiency for muons generated by GENIE, a neutrino Monte Carlo Generator, and the right plot demonstrates reconstruction efficiency for GENIE generated protons.

The SuperFGD prototype beam test has been performed at CERN in 2018, showing a clear separation of the energy deposit spectrum for proton and muon/pion samples. Electron-gamma separation and particle identification methods are also under development[23].

1.5.2 Improvements of upgraded ND280 in neutrino event selection efficiencies and interaction constraints

The upgraded ND280 has an more uniformed coverage of the high angle and backward region thanks to the upgraded detector[23]. The improvement in the event selection efficiency for charged-current inclusive muon neutrino events can be clearly seen in Figure 1.16[23].
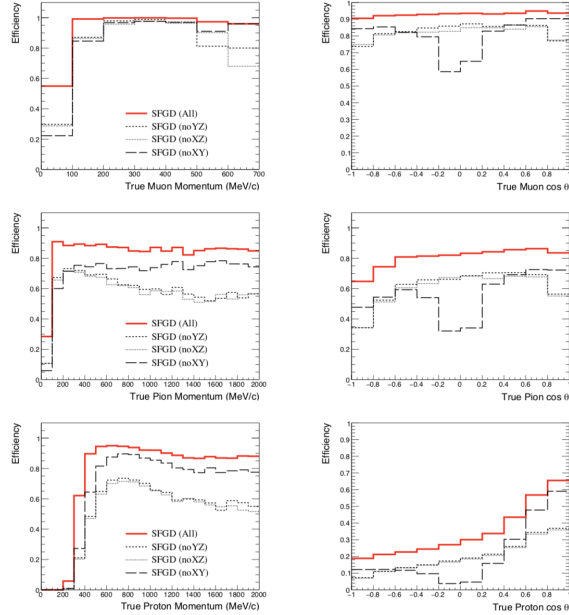
Figure 1.14: Track reconstruction efficiencies for muons and protons in Super-FGD compared to FGDXZ)[25]

Due to the large target mass, the upgraded ND280 provides about twice the selected numbers of events compared to the current configuration when the same amount of protons on target. The probability of rejecting an Out-of-Fiducial-Volume (OOFV) background event, the interaction that happened outside the fiducial volume, was estimated to be better than 95% with the TOF detector. Moreover, the purity of the selections according to final-state topologies of CC events is slightly improved.

Upgraded ND280 also aims to measure the electron neutrino cross-section, so a selection efficiency study is also done for CC electron neutrino events. The upgraded ND280 is able to detect many more electrons produced at high angles with respect to the neutrino direction, but electrons in the forward direction are less efficiently detected because they produce showers and tend to stop inside the target, as shown in Figure 1.17. Thus, the total number of selected CC electron neutrino events increases thanks to SuperFGD[23].

Based on these improvements in selection efficiencies, the upgraded ND280 is estimated to be more sensitive to SK flux normalization and better constraint cross-section parameters of interest, as shown in Table 1.1. Figure 1.18 shows the main systematic uncertainties with and without upgrade ND280. After all, we can conclude that the ND280 upgrade can lower the uncertainty for neutrino oscillation measurement.

17
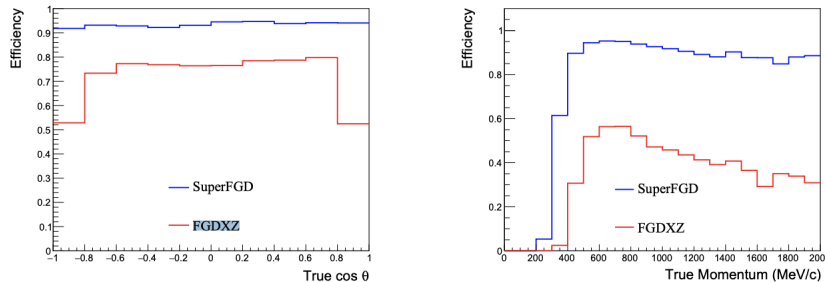
Figure 1.15: Track reconstruction efficiencies for muons, pions and protons in SuperFGD by three readout views or with two. Left plot: the reconstruction efficiency for GENIE generated muons; right plot: reconstruction efficiency for GENIE generated protons[23].

Table 1.1: Sensitivity to some flux and cross-section parameters of interest for the current ND280 and the upgrade configuration

Parameter	Current ND280(%)	Upgrade ND280(%)
SK flux normalization	3.1	2.4
$(0.6 < E_\nu < 0.7 GeV)$ MA_{QE}	2.6	1.8
ν_μ 2p2h normalization	9.5	5.9
2p2h shape on Carbon	15.6	9.4

1.6 Subject of thesis

The ND280 Upgrade detectors are currently under construction and planned to be installed in 2022. SuperFGD will utilize 56384 Multi-Pixel Photon Counters (MPPCs). Thus it is essential to check each quality before installation. Among them, 50688 MPPCs will be tested in Japan. A single setup of the test system was developed before this work as reported in [26]. In order to test a large number of MPPCs, we need to simultaneously operate multiple setups. We are planning to have eight setups in the system, and now established five of them. This thesis will report the development of five setups in the multiprocessing system and their performances.

In addition, twelve first batch of MPPC-PCBs have arrived at the University of Tokyo. We did a quality inspection on those MPPCs to check their behaviour before the mass production of MPPC-PCBs can finally start. It is a crucial step to ensure MPPC-PCBs will be expected to meet the requirement for SuperFGD. This thesis will report measurements of these MPPCs.
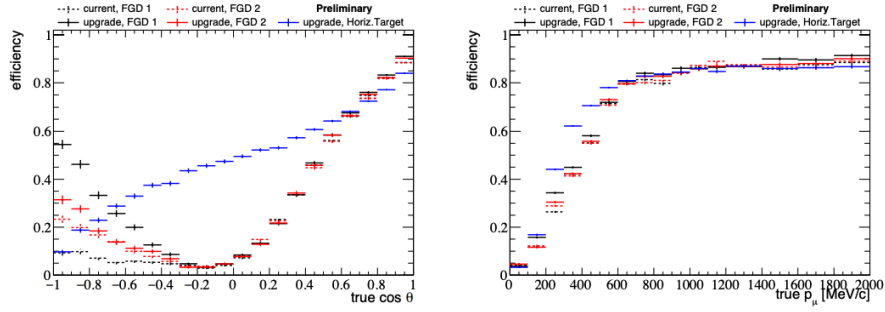
Figure 1.16: The ν_μ-CC event selection efficiency as a function of the true muon angle with respect to the z direction(left) and the true muon momentum(right) for both current and upgraded ND280 configurations[23]
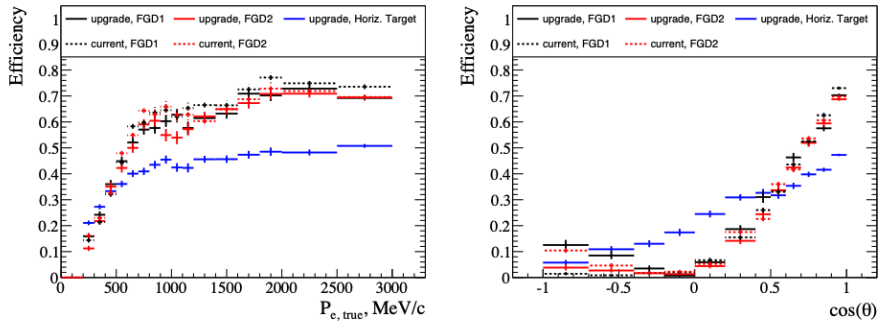
Figure 1.17: The ν_e-CC event selection efficiency with an electron detected in a TPC, as a function of the electron angle with respect to the Z direction (left) and the true electron momentum (right) for both current and upgraded ND280 configurations[23]

19
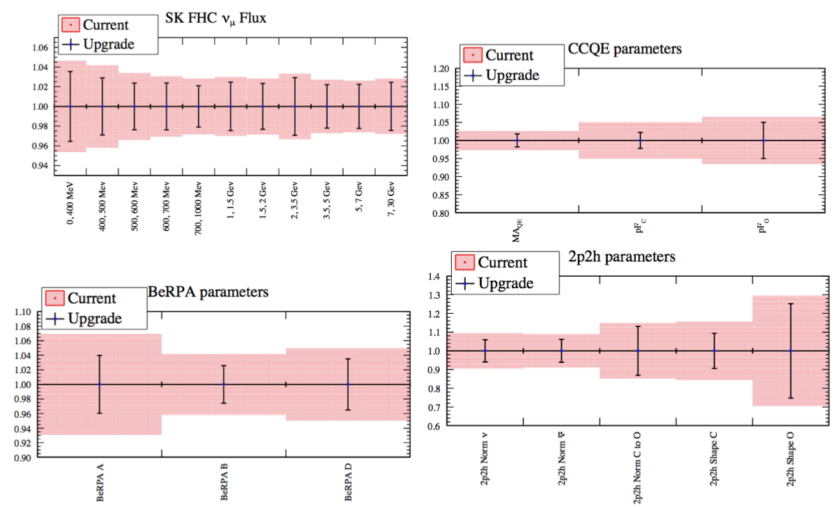
Figure 1.18: The post-fit errors on the main systematic parameters are shown for both the ND280 upgrade (blue dots) and the current ND280 configuration (red bars) [25]

Chapter 2

Multi-Pixel Photon Counter

Multi-Pixel Photon Counter(MPPC) is a type of silicon photomultiplier (SiPM), which has been widely used in high energy physics experiments. It is a solid-state photodetector that uses multiple avalanche photodiode (APD) pixels operating in Geiger mode [27]. Sixty thousand MPPC is designed to be equipped to the end of wavelength-shifting fibers for readout in the SuperFGD. T2K experiment has already established the technology to use MPPCs coupled with WLS fibers in ND280. MPPC S13360-1325PE [28], a commercial product produced by Hamamatsu Photonics K.K, is adopted for the SuperFGD [29]. The configuration of the upgrades detector requires MPPCs and their optical interfaces to be compactly arranged. Thus, T2K has developed a type of arrayed MPPCs on printed circuit board (PCB) and optical interface.

2.1 Semiconductor photon detectors

2.1.1 Photodiode

Photodiode is a semiconductor PN junction device that generates current when irradiated by light.

P-N junction

A PN junction is fabricated when negative(N) type semiconductor and positive(P) type semiconductor materials contacting with each other and creates a difference in electrical potential at the boundary [30], as shown in Figure 2.1. The region at boundaries between N-side and P-side, called depletion layer, has no electrons or holes but has an internal electric field. Intrinsically, electrons can float from the electron-excess N side to hole-excess P side. Thus, the photodiode

allows one direction electric current when valence electrons in the semiconductor activated by light and diffuse to the depletion layer, as shown in Figure 17(b).
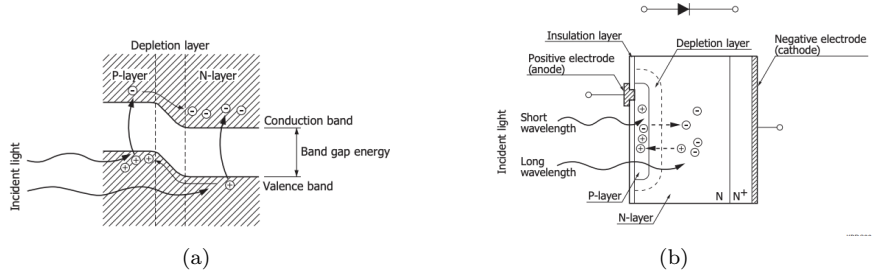
Figure 2.1: (a):PN conjunction;(b):Schematic of a photodiode cross section[30]

In general, Si photodiodes are widely used in photon detection because its excellent linearity with respect to incident light, low noise and long life.

2.1.2 Avalanche photodiode

The avalanche photodiode(APD) is a highly sensitive semiconductor photodiode that internally multiplies photocurrent during a process called avalanche multiplication. The avalanche multiplication process greatly increases the sensitivity of a p-n junction used as a photosensor and enables the measurement of low-level light signals with excellent linearity. However, Avalanche photodiodes still need some 20 photons for a detectable light pulse [31].

Avalanche multiplication

Avalanche multiplication is based on the phenomenon that high energy electron can generate further electron-hole pairs by impacting ionization when colliding with the crystal lattice. In APD, The process is based on high electric field on the order of several volts per micrometer to accelerates electrons [32]. The ionization probability is propisitional to the electric field.

The way of generating primary electrons in the APD is same as in photodiode. In addition electric field in APD can accelerate the electron to a certain energy level that avalanche multiplication occurs, as shown in Figure 2.2.

2.1.3 Geiger-mode avalanche photodiodes

Geiger-mode avalanche photodiodes have been developed during recent years, being an alternative to photomultiplier tubes. They enable single-photon response, and thus high detection efficiency, and also high gain at low bias voltage. However, they also have features that might cause problems, such as the dark count rate [31].
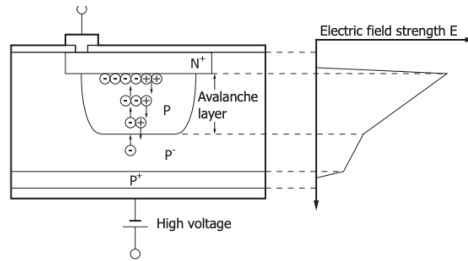
Figure 2.2: Schematic diagram of avalanche multiplication(near infrared type) [33]

Geiger mode and quenching circuit

The Geiger mode avalanche photodiodes have a structure allowing operation without damage under a bias voltage which is well above its reverse-bias break-down voltage. Thus the ionization level in the photodiodes is high and thus enable one photon detection. Its output pulses indicate a trigger and can be likened to Geiger-counter and therefore called "Geiger-mode". At the operation bias, the electric field is so high that a single charge carrier injected into the depletion layer can trigger a self-sustaining avalanche [34]. The current rises swiftly and continues to flow as long as the electric field keeps still. Thus, the avalanche should be quenched in order to halt the Geiger discharge, which can be done by an external circuit lowering the bias voltage. And then, a second photon can be detected when the bias voltage to being restored.

2.2 Multi-pixel photon counter

As discussed, the multi-pixel photon counter(MPPC) uses multiple APD pixels operating in Geiger mode, as shown in Figure 2.3. It can be used for detecting extremely weak light at the photon counting level with excellent time resolution [33]. Each pixel in the MPPC outputs a signal at the same amplitude when detecting a photon, and pulses generated by multiple pixels are superimposed onto each other. Thus the height of output pulses demonstrates the number of detected photons. For example, four photons result in a pulse height equal to four times a single-photon pulse height. On the other hand, each pixel of the MPPC cannot distinguish the number of the entering photons. Thus, the linearity of the MPPC get worse when confronting more arriving photons, so it is essential to have enough pixels to match its designed usage. Intrinsically, the number of the incident photons can be estimated from observing the pulse height on the oscilloscope, shown in 2.4a, and measuring the output charge, which can be integrated and plotted as a "finger plot", as indicated in 2.4b [33].
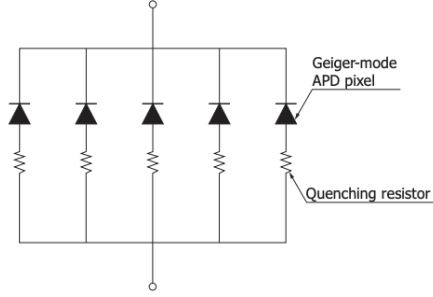
Figure 2.3: Schematic of Geiger Mode acalanche photodiodes and quenching circuit)[33]

(a)

(b)
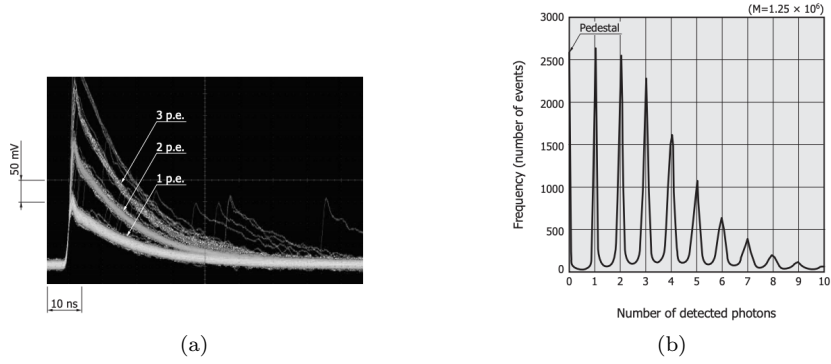
Figure 2.4: (a): Pulse waveforms when using a lnear amplifier(120 times)(S12571−050C M=1.25 × 10^6);(b): Pulse height spectrum when using charge amplifier (S12571-050C M=1.25 × 10^6)[33]

2.2.1 Characteristics

Gain

The MPPC gain is defined as the ratio between output charge(Q) of one photon to the electric charge($q = 1.602 \times 10^{-19} C$), as

$$M = \frac{Q}{q}. \tag{2.1}$$

The charge Q is linearly proportional to the over voltage, defined as the difference between bias voltage and breakdown voltage.

$$Q = C \times (V_{bias} - V_{br}) = C \times V_{over}, \tag{2.2}$$

24

where C as the capacitance of one pixel, V_{bias} as the bias voltage, V_{br} as the breakdown voltage, and the over voltage defined as $V_{over} = V_{bias} - V_{br}$.

Making use of the APD, the MPPC also has a temperature dependence. The crystal lattice vibrates stronger at the higher temperature, increasing the probability of carriers striking the crystal before the energy reaches the ionization level, thus suppressing ionization. Typically, in order to attain constant gain, bias voltage should rise linearly as ambient temperature increase. The temperature dependence of the breakdown voltage is typically about 50 mV/degree.

Dark noise

In the MPPC operation, pulses can be generated by both photon-generated electrons and thermally-generated electrons. The thermally generated electron pulse, called dark pulse, are unwanted in photon detection and causing errors. However, those dark pulses undergo the same procedure as photon-generated ones and cannot be distinguished. The thermally-generated pulse has a temperature as suggested by its cause, which can be described as:

$$N_{0.5p.e.}(T) \approx AT^{\frac{3}{2}} e^{\frac{E_g}{2kT}}, \tag{2.3}$$

where:
$N_{0.5p.e.}$ as the dark count rate, the number of dark pulse generated in a dark state and exceed a threshold of 0.5p.e in one second;
T as the absolute temperature[K];
A as arbitrary constant;
E_g as band gap energy[eV];
k as Boltzmann's constant[eV/K].

Cross talk

Optical crosstalk happens when secondary photons are generated in the avalanche multiplication process and detected by other pixels. It causes a pulse of 2 p.e. or higher when photons enter only one MPPC pixel. The cross-talk probability can be defined as the ratio of the dark noise rate measured with a 1.5 p.e. threshold to that measured with 0.5 p.e. threshold, as

$$P_{cross-talk} = \frac{N_{1.5p.e.}}{N_{0.5p.e.}}. \tag{2.4}$$

The crosstalk probability has very low dependence on the temperature at fixed bias voltage within the range of operating temperature, but increase as the over voltage increase.

Afterpulse

Afterpulse happens when the generated carrier gets trapped by lattice defects and then released and multiplied in avalanche processes. It cannot be distinguished from the photon-generated pulse.

Photosensitivity and photon detection efficiency

Photosensitivity and photon detection efficiency describe MPPC's ability to detect light.

Photosensitivity (S) can be expressed as the ratio of the MPPC output current (I_{MPPC}: photocurrent[A]) to the amount of continuous light incident on MPPC

$$S = \frac{I_{mppc}}{\text{Incident light level}}.$$ (2.5)

The photosensitivity is proportional to the gain and thus a higher bias voltage results in higher photosensitivity, which does not exclude crosstalk and afterpulse.

Photon detection efficiency(PDE) is the ratio of the number of detected photons to the number of incident photons when light enters the MPPC:

$$PDE = \frac{\text{Number of detected photons}}{\text{Number of incident photons}}.$$ (2.6)

PDE can be expressed as:

$$PDE = Fg \times QE \times Pa,$$ (2.7)

where:
Fg is the fill factor which is the ratio of the light detectable area to the entire pixel area of an MPPC, as MPPC photon-sensitive area contains sections such as the inter-pixel wiring that cannot detect light;
QE is the quantum efficiency, defined as the probability that carriers being generated by light incident on a pixel, which depends on light wavelength;
Pa is the avalanche probability that generated carriers cause avalanche multiplications, which gets higher when bias voltage increases.

2.3   MPPC adopted for SuperFGD

As discussed before, the upgraded detector will be installed in the upstream of TPC/FGDs, replacing P0D. Thus, to fit in the space, the MPPC and electronics need to have a compact design. ND280 upgrade group chooses to adopt surface-mount type MPPC S13360−1325PE, produced by Hamamatsu Photonics K.K to superFGD. Dimension of the photosensor is 2.625 mm × 2.1 mm × 0.85 mm and size of the photosensitive area 1.3 mm × 1.3 mm. Compared to the current ceramic type used in ND280, this type has a smaller package size and thus mechanically enables compactness and enough optical coupling with 1 mm diameter WLS fiber. Besides, the dark count rate and cross-talk probability are much lower than the MPPC currently used in ND280. This type of MPPC operates at room temperature and operate under low voltage operation. A typical breakdown voltage is 51 volt. It is recommended to work under the overvoltage equals to 5V. Other characteristics can be seen in Table 2.1.

Table 2.1: MPPC(S13360-1325PE) Characteristics [28]

Item	Specification
Photosensitive area	1.3 mm × 1.3 mm
Pixel pitch	25 μm
Number of pixels	2668
Fill factor	47%
Package	Surface mount
Breakdown voltage	53±5 V
Peak sensitivity wavelength	450 nm
Photon detection efficiency	25%
Gain	7.0×10^5
Dark Noise rate	70 kHz
Crosstalk probability	1%
Operating temperature	-20 to 60 °C
Storage temperature	-20 to 80 °C

MPPCs are designed to be installed on the SuperFGD box, the supporting structure that holds SuperFGD. WLS fibers are individually inserted into scintillator cubes from holes in the box. Figure 2.5 gives the design of the SuperFGD MPPC-PCB and the optical interface.
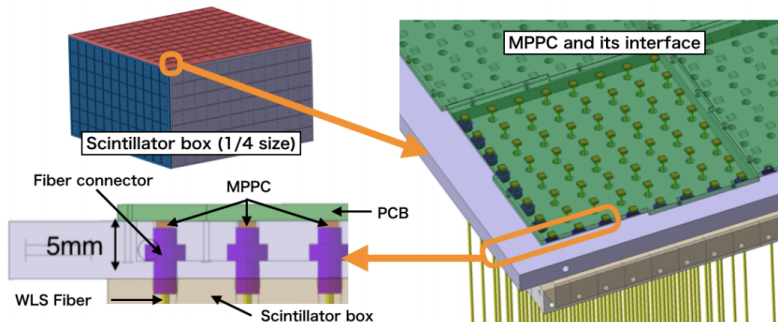
Figure 2.5: Design of MPPC-PCB and the optical interface. [29]

2.3.1 MPPC-PCB

MPPCs are 8×8 arrayed on 8 cm×8 cm PCB boards. MPPCs are integrated into front sides of PCBs, as shown in Figure 2.6(a). For each MPPC, a 1kΩ resistor and a $0.1\mu F$ capacitor are installed as a low-pass filter on the backside

of the PCB. There are two temperature sensors(103KT-1608T-1P) mounted on the backside for temperature monitoring. The readout port(LSHM-140-02.5-L-DV-A-S-K-TR) also locates at the backside of the PCB, which provides the bias voltage and readouts the signals from 64 MPPCs and temperature sensors.

(a)   (b)
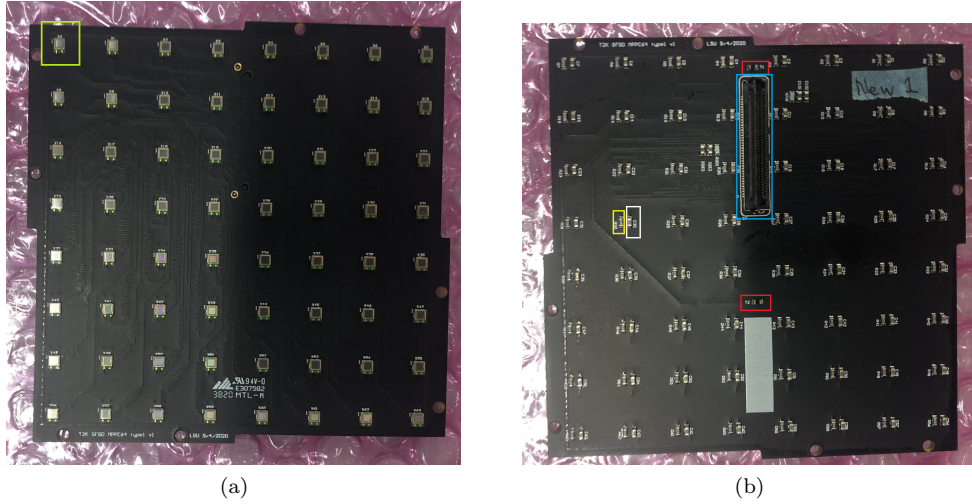
Figure 2.6: (a): Front side of the MPPC-PCB. The green box highlights a single mppc. (b): Back side of the MPPC-PCB. Red boxes: two temperature sensors; blue box: port; yellow box: Resistor; white box: Capacitor

2.3.2   MPPC requirements for SuperFGD

In order to ensure the SFGD ability and control the systematic errors, it is crucial to have the MPPCs meet certain quality requirements [26].

Gain and PDE

Gain is in the very upstream of the analysis flow. Also, the uniformity of the gain and PDE is crucial in the SuperFGD based particle identification. The SFGD prototype beam test in 2018 checked the uniformity of the readout channel, as shown in Figure 2.7. The light yield produced by minimum ionization particles is checked for all 384 channels in the prototype and calculated using four different calibration methods shown as different lines.

All calibration methods suggest a variation of approximately 25%. This variation comes from the non-uniformity of gain and PDE and other factors such as defects and failures of fibers, scintillator cubes, connection defect. Thus, the variation of gain and PDE is considered to be less than 25%. Other studies on the other S13360 MPPCs [36] used in T2K near detector suggested that the gain range is about $\pm 12\%$ and the standard deviation is about 3.8%, and relative PDE range is about $\pm$ 10% [37].
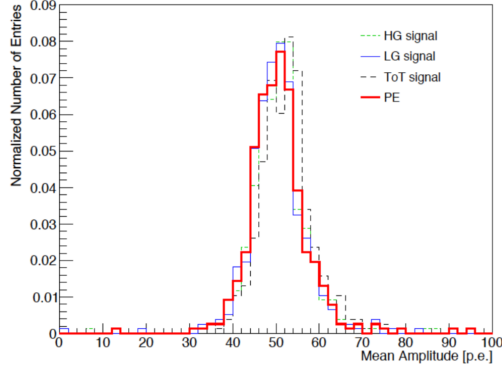
Figure 2.7: Mean light yield produced by minimum ionizing particles for 384 readout channels of the prototype of SuperFGD [35]

In conclusion, the gain under typical working voltage should be within about ±12% range and the PDE under typical working voltage should be within about ±10% range. Furthermore, 12% variation corresponds to about 0.6V of operation voltage. Thus, in SFGD operation gain tuning, applying different voltages to each MPPC can further reduce the variation.

Operation Voltage

As mentioned, it is possible to adjust apply different voltage to each MPPC for gain tuning in SuperFGD operation. The range of this adjustment is 2.5V, which means the variation of the breakdown voltage for all MPPC should be lower than 2.5V to realize gain tuning. Hamamatsu delivered 768 MPPCs in a reel and measured the operation voltage before render MPPC, defined as 5V over breakdown voltage, and results are shown in Figure 2.8. According to Hamamatsu measurement, the variation of operation voltage of all MPPCs used is within 2.5V. Furthermore, the variation of the operation voltage in each reel is within 0.3V. After all, the variation is expected to meet the requirement of the gain tuning.

Dark Count and Cross Talk

Dark count and cross talk are both unwanted counts, mistakenly measured as real hits in photon detection. Thus it is important to understand the dark count rate and crosstalk probability. We set the dark noise rate requirement to be under 200 kHz, and crosstalk probability requirement to be less than 3%. If requirements being fulfilled and level threshold set to 1.5 p.e., given that T2K has a lot of time width of about 50 ns, and that hits are counted only all three directions detects a signal, the noise hit is negligibly small in SFGD.
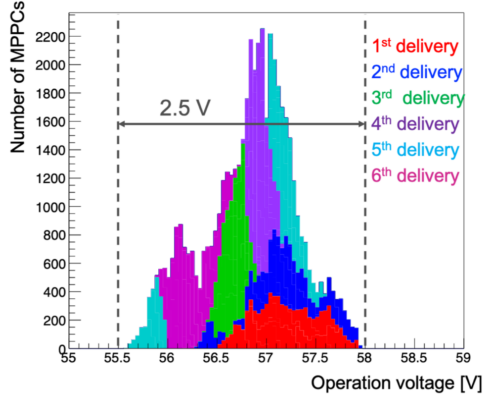
Figure 2.8: Operation voltage measured by Hamamatsu [26]

In summary, the requirements of the characteristic of the MPPC can be seen in Table 2.2.

Table 2.2: Requirements of the MPPC Characteristics

Item	Requirements
Gain	variation $\leq 12\%$
Relative PDE	variation $\leq 10\%$
Breakdown voltage	variation ≤ 1.25 V in each PCB
Dark Noise rate	≤ 200 kHz
Crosstalk probability	$\leq 3\%$

2.4 Production, render and mass test

There are in total 56384 MPPCs designed to be used for SuperFGD. Hamamatsu Photonics has finished producing all MPPCs and delivered 50688 MPPCs in Japan and other 10k MPPCs to the United States. 768 MPPCs are packed in reel for delivery. SuperFGD will make use of 881 MPPC-PCBs, 792 of which will be produced and tested in Japan. The first batch of MPPC-PCB has been tested as described in Chapter 5.

Chapter 3

Design of the MPPC Performance Test System

Hamamatsu Photonics gives typical values of MPPCs in their documents [26] and measured value before each delivery. SuperFGD will make use of 881 MPPC-PCBs, 792 of which will be produced and tested in Japen. However, Hamamatsu does not provide operation voltage for each MPPC, just the range of the measured operation voltage. Moreover, due to the large number of MPPC used, it is very hard to track each MPPCs in the delivery and PCB production stage. Thus, we will carry out a quality test before MPPC-PCB being installed to SuperFGD to assess MPPC-PCB behavior and provide data for SuperFGD tuning. We aim to check gain, breakdown voltage, operation voltage, relative PDE, dark noise rate, and cross talk. Here we define the operation voltage as the voltage gives a gain of 5.0×10^5. A mass test system that enables eight parallel tests of eight MPPC-PCBs at the same time is under development. In order to confirm that MPPCs meet the requirements discussed in Subsection 2.3.2, measurement uncertainties of the test system should also meet certain criteria, as shown in Table 3.1.

Breakdown voltage is also measured during the test, but in general, the uncertainty of the breakdown voltage will be larger than that of operation voltage because of the analysis process. Thus, we use the operation voltage to evaluate the variation of the voltage behavior of MPPC.

Table 3.1: Requirements of the uncertainty of the test system

Item	Requirements of uncertainty
Gain	$< 3\%$(ratio)
Operation voltage	< 0.1 V
Relative PDE	$< 3\%$(ratio)
Crosstalk probability	$< 0.1\%$
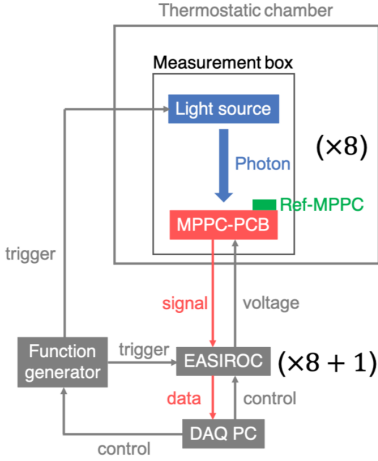
Figure 3.1: A schematic view of the test system[26]

3.1 Overview

There are eight identical test sets to measure eight MPPC-PCBs in each run. Each set includes a measurement box, holding light source and MPPC-PCB, signal reading out system (NIM EASIROC modules) and data acquisition (DAQ) PC. As many MPPC characteristics have a temperature dependence, the measurement box is kept in the thermostatic chamber. The light source and NIM EASIROC is triggered by the function generator. The DAQ PC communicate with both the function generator and EASIROC. The schematic view of the test system is shown in Figure 3.1. There is also a fixed reference MPPC inside each measurement box for light monitoring.

3.2 Hardware construction

3.2.1 NIM EASIROC module

NIM EASIROC (Extended Analog Silicon PM Integrated ReadOut Chip) is a general-purpose MPPC readout module developed by the OpenIt project [38]. As shown in Figure 3.2, EASIROC has 64 MPPC input channels. Each of the two chips provides voltage and reads signals for 32 channels. Figure 3.3 shows the block diagram of EASIROC. The bias voltage applied to each MPPC can be individually adjusted within the range of 4.5 volts by 8 bit "input DAC". Monitor ADC monitors the bias voltage at the same time. The input signal is divided into two pre-amplifiers, one with high gain adjustable from 10 to 150 and the other one with low gain adjustable from 1 to 15 [38]. The signal of the
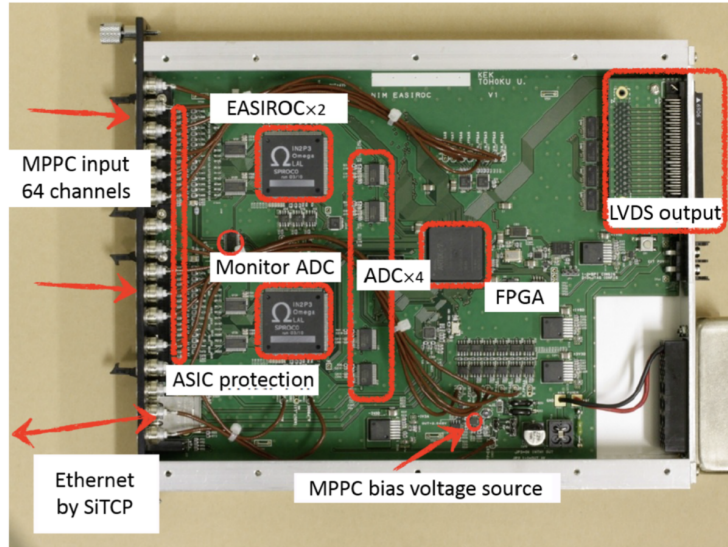
Figure 3.2: A schematic view of the test system [26]

high gain preamp is further sent to slow shaper for energy measurement and fast shaper for a logic generation. A discriminator after the fast shaper determines if the pulse height exceeds a given common threshold for all channels, chosen by 1.3 V/10 bit "threshold DAC". Slow shaping time can be adjusted between 25 and 175 ns for both low and high gain. The pulse height is sampled and held by an external hold signal and stored in analog memory. Then the held 32 signals are multiplexed and read out. A field-programmable gate array (FPGA) controls the configuration of the EASIROC chip and data acquisition. Data exchange between FPGA and DAQ PC is done through Ethernet [39]. The bias voltage, the voltage of input DAC, the threshold voltage of the discriminator, and the timing of the HOLD signal are controllable from DAQ PC[26].

There will be nine NIM EASIROC modules used in the test, eight of which reads signals from the MPPC-PCB. The rest is designed to read out reference MPPC.

3.2.2 Light source

An array of LED (NSPB300B, Nichia) is used as the light source[40] when measuring gain and relative PDE. LEDs have wavelength peaks at 465 nm, which is close to the sensitivity peak of measured MPPC (about 450 nm) and emission peak (476 nm) of the WLS fiber. A light guide plate and a white glass diffuser are placed in the direction of photon propagation to ensure light uniformity inside the measurement box. The light guide is a 10 cm × 10 cm acrylic plate with notches in 1 cm × 1 cm interval. The diffuser diffuses light
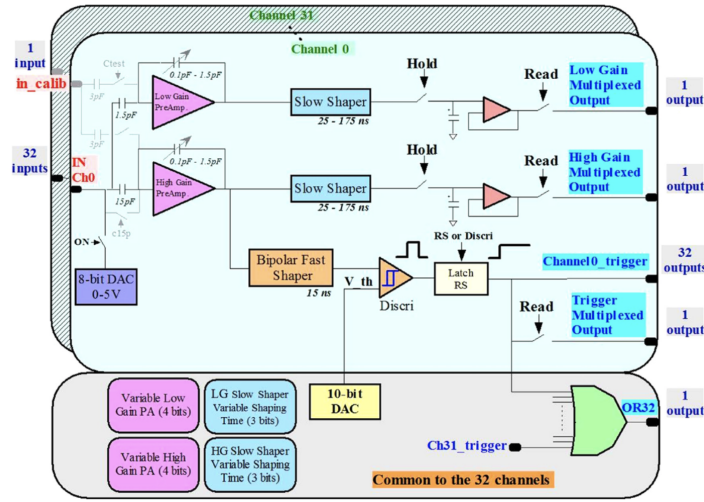
Figure 3.3: A block diagram of EASIROC [38]

with wavelengths of 400-700 nm by the Tyndal scattering. A schematic view of the light source and a photo of the light source is shown in Figure 3.4 [26]. LEDs are controlled by a function generator and the luminosity can be adjusted by changing pulse width.

The LED array are fixed to the measurement box and connected to the function generator through an intermediate board, as shown in Figure 3.5. The interface board are covered with aluminium foil to reduce electromagnetic noise during the test.

| | |
| (a) | (b) |
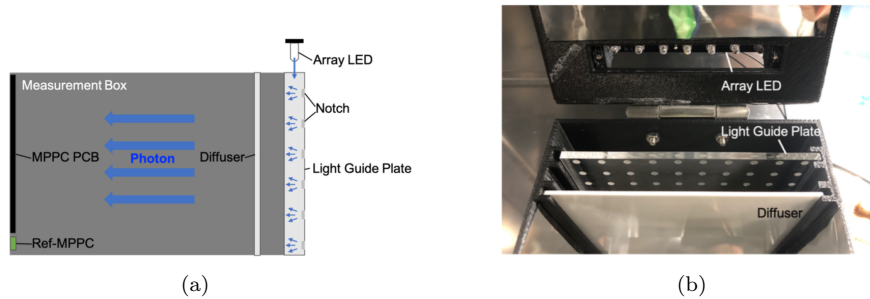
Figure 3.4: (a): A schematic view of the light source); (b): A photo of the light source
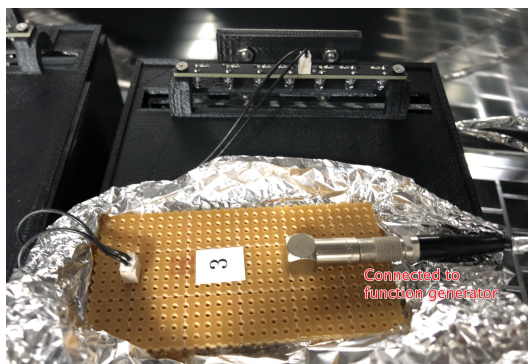
Figure 3.5: LED fixed to the measurement box

3.2.3 Measurement box

The measurement box is a plastic box of size 11 cm × 10 cm × 30 cm which will hold MPPC-PCB, reference PCB and light source. As shown in Figure 3.6, it will be open to exchange MPPC-PCB and close when taking measurement. The MPPC-PCB and the reference MPPC will be held at one end of the box, and the light source locates in the other. Mirror sheets cover the inner wall of the box to improve light uniformity.

3.2.4 Thermostatic chamber

Two thermostatic chambers are used in the test. One is type INE800 Yamato, referred as Chamber 1, and the other is FMU-204I Fukushima, referred as Chamber 2. Chamber 1 is holding three of eight measurement boxes while chamber 2 holding the rest five. The picture of the two chamber is shown in Figure 3.7 [26].

3.2.5 Reference MPPC

A reference MPPC (S13081-050CS) is installed to monitor light for measuring relative PDE for each test set. Features of this type is summarized in Table 3.2. The bias voltage of the MPPC is fixed at 52.5 V in test. Photos of reference MPPC and its holder is shown in Figure 3.8.

3.2.6 Cables and interface board

The MPPC-PCB in measurement is connected to an intermediate board through a flat cable. The cable is wrapped with aluminium tape to be shielded from electromagnetic noise. The wire end closed to the MPPC-PCB is covered with plastic tape to avoid a potential short circuit when multiple cables are placed in the chamber. The intermediate board then divides 64 channels into

Figure 3.6: A measurement box.(a):Diffuser; (B) Light Guide; (C) LED array; (D) MPPC-PCB(a reference mppc fixed below the PCB but cannot be seen in this picture); (E)Lid

two wires, each including 32 channels, and connected to the EASIROC module by two flat cables. All eight reference MPPCs are connected to one intermediate board by aluminium-wrapped coaxial wires, and then the intermediate board is connected to EASIROC by flat cable, as shown in Figure 3.9a. The end part of the wire is wrapped by plastic tape to avoid a short circuit. The cables and intermediate board is shown in Figure 3.9b and Figure 3.9c. The arrows in Figure 3.9 demonstrate the direction of signal flow.

3.2.7   Parallel measurement

Eight measurement sets are constructed with the same design. the electromagnetic noise gets larger when more settings adding to the testing area. Thus, it is necessary to ground cables and use more shielding. The eight EASIROCs and intermediate boards are held together on the iron shelf, as shown in Figure 3.10b. Chamber 2 is placed to the left of EASIROCs and holding five measurement boxes, as shown in Figure 3.10a. Chamber 1 is placed to the right of EASIROCs and holding three measurement boxes, as shown in Figure 3.10c. The measurement boxes in chamber 1 will be covered with the black sheet to improve thermal stability during the test.

<div align="center">(a)   (b)</div>
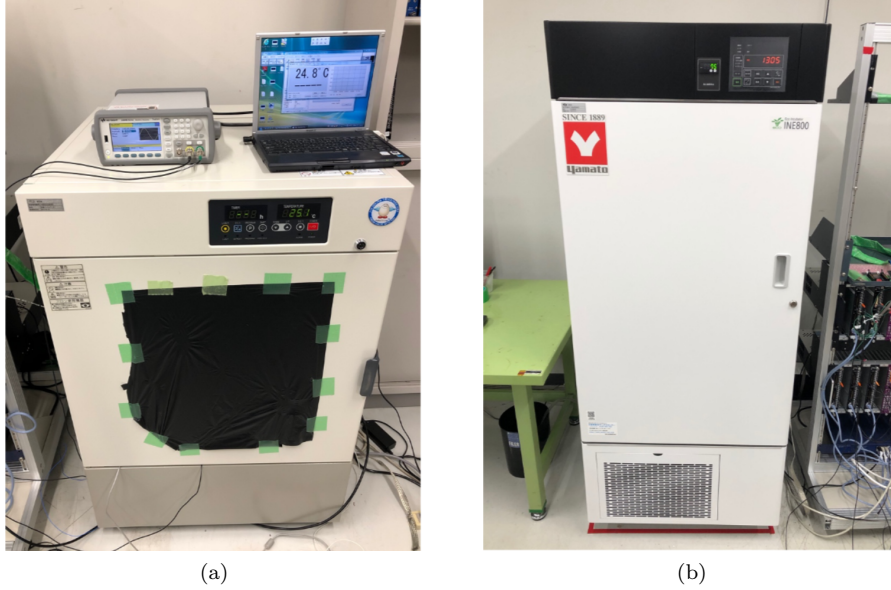
Figure 3.7: (a): Chamber 1); (b): Chamber 2

3.3 Measurement method

3.3.1 Tuned parameters of EASIROC

HOLD timing

The EASIROC measures the pulse height of an MPPC by memorizing the voltage of a slow shaper signal at the timing when a HOLD signal arrives. Thus, it is important to tune the HOLD timing that matches the peak timing of the MPPC signal. In order to do so, measurements were done for a range of HOLD timing and then fitted by a quadratic function. Figure 3.11a shows a typical HOLD timing scan and fit. The chosen value is determined to be which maximize the signal height. For each EASIROC module, the HOLD timing for one module is defined to be the mean of the distribution of 64 channels, as indicated in Figure 3.11b . For each module, the HOLD timing is measured and fixed during the performance test.

Charge-ADC calibration

A calibration between charge and ADC digital value was done by using test pulse. The ADC value and injected charge can be fitted by a linear function. The conversion factor from ADC to injector charge F_{calib} is defined as the slope of the linear function, as shown in Figure 3.12 [26].

Considering that amplification rate of the high gain preamp is 30 for test

Table 3.2: MPPC(S13081-050CS) Characteristics [28]

Item	Specification
Package	Ceramic type
Photosensitive area	1.3 mm × 1.3 mm
Pixel pitch	$50 \times 50 \ \mu m^2$
Number of pixels	667
Operation voltage	54.5 V
Peak sensitivity wavelength	450 nm
Photon detection efficiency	35%
Gain	1.5×10^6
Dark Noise rate	90 kHz
Crosstalk probability	1%

(a) (b)
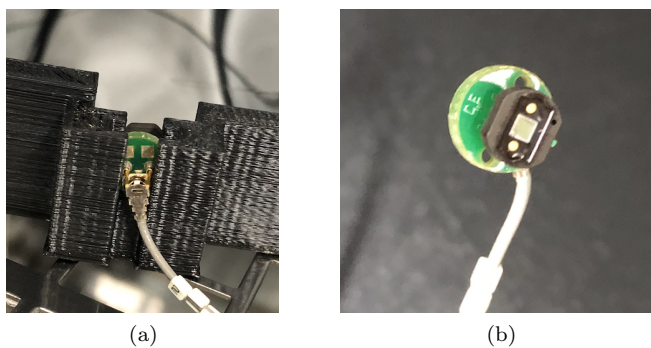
Figure 3.8: (a): Reference MPPC installed to the measurement box 1); (b): Front side of the reference MPPC

charge and 150 for MPPC, the conversion factor for MPPC F_{MPPC} can be scaled by $\frac{30}{150}$, as

$$F_{MPPC} = \frac{1}{5} F_{calib}. \tag{3.1}$$

Threshold DAC

MPPC signals exceeding a certain threshold are counted in EASIROC operation. Thus, it is important to decide its own threshold DAC for each chip of EASIROC. This threshold level are tuned to corresponds to 0.5p.e. level as the measurement of dark noise rate has the threshold of 0.5 p.e. level. The measurements of noise rate are taken with respect to changing threshold DACs at a constant voltage of 55.5V. The relationship between noise rate and DAC

can be fitted by a sum of two sigmoid functions and a constant, as shown in Figure 3.13

The bias voltage is higher than 55.5V during the performance test. Thus, the parameter tuned at 55.5V will not underestimate the noise rate in the performance test because the gain of an MPPC increases as the bias voltage increases. On the other hand, the gain is smaller at the fixed voltage for an MPPC-PCB which has a higher breakdown voltage. As a result, its noise rate will be underestimated if the same threshold level is applied.

Temperature calibration

The two temperature sensors in the PCB board can be used to monitor the PCB temperature. The voltage read by the temperature sensor and output to a certain value. We calibrate this value to temperature reading in $^{\circ}C$ by an external thermal recorder(TR-712U, T&CORP). The recorder sensor is placed near the PCB sensor1 to monitor the ambient temperature. While the PCB temperature changes slower than the area temperature, we need to wait for another 40 minutes for the PCB sensor measured value to stabilize. The measurements are done for different ambient temperatures in the interval of $1^{\circ}C$. We use the reading from the external temperature recorder as the trusted value for the PCB temperature. Readings can be fitted separately for two sensors on the PCB to a linear function, as shown in Figure 3.14.

The study was done using one PCB and it is found that the fitting parameters differs little between each sensors and EASIROC modules, but this discrepancy can be corrected by a linear shift. The reading are calibrated by one PCB and fitting parameters are treated as the same in each measurement trial of each EASIROCs during the mass test.

3.3.2   Measurement flow and DAQ

The main measurement takes about 32 min for each PCB. However as the PCB board will be replaced manually, which might cause a connection problem so a pre-check test for the connection is considered. In this section, the measurement flow and DAC setting at each stage for the test is discussed.

Pre-check test

The pre-check test aims only to confirm that the connection is fine to get ready for the main test, and its data is not used in data analysis. Thus, it includes one fixed voltage ADC measurement while LED is on, using the DAQ external trigger rate of 2 kHZ at 55 V. As long as the ADC distribution shows the ADC reading is normal for all PCBs in the test and the reference MPPC, the pre-check allows the main test to start. Also, an electromagnetic background noise check for all settings except the reference MPPCs setting is also done during the pre-check. The system read the noise rate at zero volt bias voltage applied to the MPPC with LEDs emitting no light but function generator sending out

a trigger. Figure 3.15 shows a typical ADC 2D plot and a typical background noise 2D plot. In the ADC plot, it can be clearly seen that there are stripes corresponding to peaks in the ADC single channel plot. For background noise we check the scaler data. If the noise is lower than 5 kHz then it is fine to proceed to the main test. During the mass test, the background noise condition is expected to be stable but if the background noise condition changed it is necessary to suppress noise before starting the main measurement.

Main test

There are three stages of the main test, which separately measures ADC, dark noise rate and s-curve.

In the ADC mode, the ADC distribution is measured. The LED is turned on, and the external trigger rate of DAQ is 2 kHZ. ADC data are taken from 55.5 V to 57.4 V in an interval of 0.1 V. It takes 20 seconds to measure 40,000events for each voltage, and thus the total time of ADC measurements about 9 minutes.

Dark noise mode measures scaler data from which dark rate can be calculated. In this stage, LED is off. Scaler data is taken under twenty bias voltages from 55.5 V to 57.4 V in the interval of 0.1V at a fixed threshold level of 0.5 p.e.. Each measurement at certain voltages takes 10 seconds, and the total time cost of dark noise mode added up to 5 minutes.

S-curve mode also measures scaler data while the LED is turned off. At this stage, measurements are performed under the bias voltage of 55.5 V, 56.0 V, 56.5 V and 57.0 V, with threshold DAC changing at each voltage. The total time for s-curve measurement is about 18 minutes.

3.3.3 The testing procedure and multi-processing

Measurements for eight settings are done in the same way, but several parameters are different. Eight threads of the DAQ PC control eight measurements. The data analysis, which is quick compared to measurements, is done in a queue. The measurement progressing time has been confirmed not being slowed down for parallel setting compared to a single setting.

The whole testing trial of one group of MPPC-PCB takes more than one hour. First, we install the MPPC-PCBs in the measurement box and then run the pre-check test. After the pre-check confirms the connection is ready for the main test, we wait for 40 minutes for the temperature to stabilize to $20^\circ C$ and then start the main test. We check the quality of the main test after measurement finished and changes MPPC-PCB. Data analysis is quick and can be done during the waiting, which will be discussed in Section 3.4.

3.4 Analysis methodology

We analyse data after all three measurements are completed. In this section, the analysis methodology is discussed.

3.4.1 ADC mode

The ADC mode provides ADC distributions at different bias voltages for each channel while LED is on. From those data, we can calculate gain, operation voltage, breakdown voltage, and relative PDE.

Gain

A typical ADC distribution looks like a finger graph, as shown in Figure 3.16a.

Peaks in the ADC distribution corresponds to 0p.e. events, 1p.e. events, and so on. The peak can be found by fitting the distribution with double Gaussian. The 1 p.e. level pulse-height(H) of MPPC is defined as the numerical difference of the ADC counts between 0 p.e. and 1 p.e peak. Thus gain can be calculated as:

$$Gain = \frac{Q}{e} = \frac{F_{MPPC} \times H}{e}, \tag{3.2}$$

where F_{MPPC} is the conversion factor, and e is the elementary charge.

Operation Voltage and breakdown voltage

The operation voltage is defined as the voltage which gives a gain of 5.0×10^5. As measurements are taken under various voltage in ADC mode, we can plot the relation between gain and bias voltage which can be fitted to a linear function as shown in Figure 3.16b. Thus, we can calculate the operation voltage from the fitted function. Breakdown voltage is the voltage where the ADC gain is zero, which can be similarly calculated from the gain-bias fit as the operation voltage.

Relative PDE

The relative PDE is defined as the ratio between the number of photons detected by each MPPCs to the number of photons detected by the reference MPPC. Assuming the number of detected photons follows the Poisson distribution, the probability that n photons are detected by the MPPC, demonstrated by P_n is:

$$P_n = \frac{\lambda^n}{n!} e^{-\lambda}, \tag{3.3}$$

$$\lambda = -\ln P_0, \tag{3.4}$$

where P_0 can be calculate as the ratio between numbers of 0 p.e. events and the number of total events, and λ is thus the mean value of the number of the photons detected by the MPPC.

PDEs of eight reference MPPCs has checked by Haruto Kikutani [26] to be close enough to be considered. The uncertainty of the relative PDE measurement is considered to be 1%.

3.4.2 Dark noise mode

The dark noise rate is measured when LED is turned off. The threshold is tuned to be 0.5 p.e., as mentioned. The dark noise is calculated as the mean value of the distribution of 0.1 seconds measurement, as shown in Figure 3.17.

3.4.3 Cross talk mode

The optical cross talk probability is defined as the ratio of the dark noise rate (DR) with 0.5 p.e. and 1.5 p.e. level threshold in the s-curve as:

$$\text{Crosstalk Probability} = \frac{DR_{0.5p.e.}}{DR_{1.5p.e.}}. \tag{3.5}$$

A typical s-curve is given in Figure 3.14, and can be fitted with a double sigmoid function.

3.4.4 Summary

For each channel, gain, number of the photon detected, noise rate and cross talk increase as the over-voltage increase, and can be fitted as a linear function, as shown in Figure 3.18.
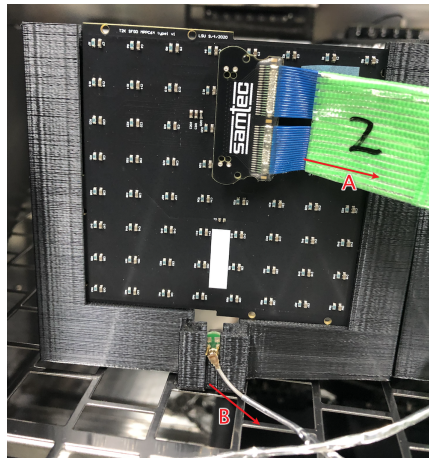
(a)
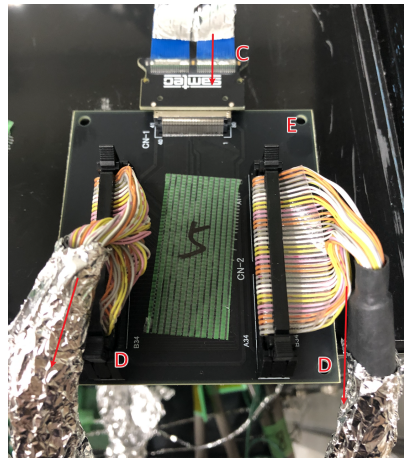
(b)

(c)

Figure 3.9: (a):C ables connected to MPPC-PCB and the reference mppc [A: flat cable connecting MPPC-PCB; B: coaxial cable connecting to MPPC]; (b): intermediate board of MPPC-PCB [C:flat cable connecting from MPPC-PCB; D: flat cable connecting to EASIROC; E:intermediate board]; (c): intermediate board for reference MPPC [F: coaxial cable connected from reference MPPC; G: flat cable connecting to EASIROC.]
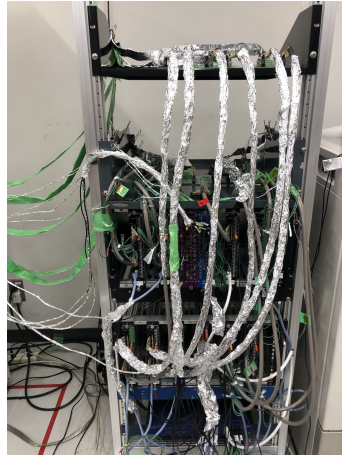
Figure 3.10: (a): Inner look of Chamber 2; (b): EASIROCs and intermediate boards; (c): Inner look of Chamber 1
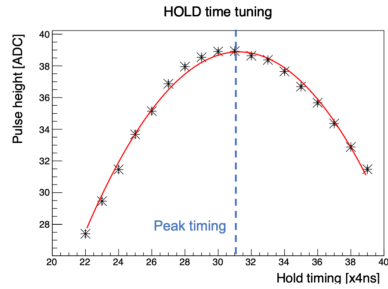
(a)
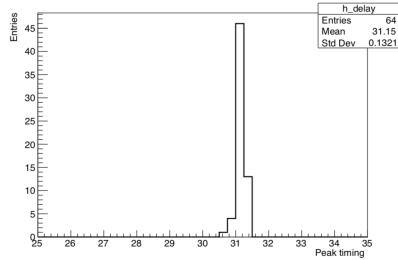
(b)

Figure 3.11: (a): A typical HOLD timing scan for one channel 1);(b): Distribution of the HOLD timing for 9 EASIROCs
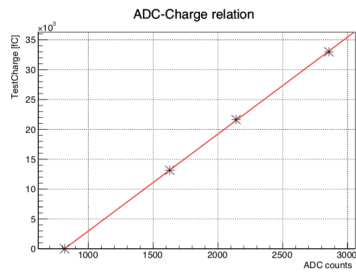
Figure 3.12: A typical Charge-ADC calibration

45
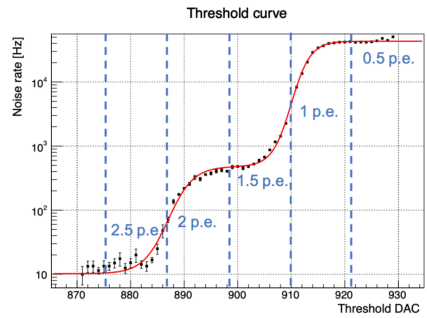
Figure 3.13: A typical Threshold DAC calibration
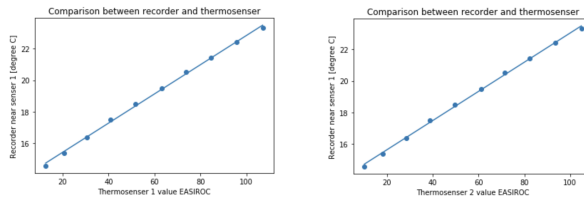
Figure 3.14: Calibration fit for sensor 1 and sensor 2
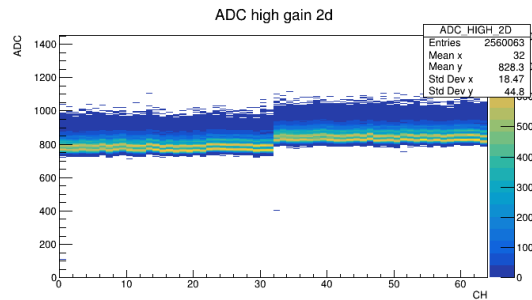
(a)
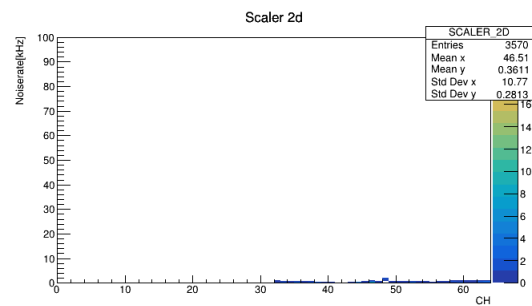
(b)

Figure 3.15: (a): A typical ADC 2D plot; (b): A typical SCALER 2D plot
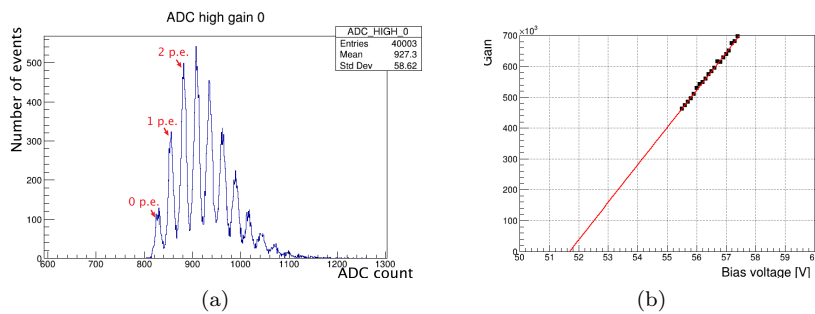
(a)

(b)

Figure 3.16: (a): ADC distribution 1); (b): Gain as a function of biased voltage

47
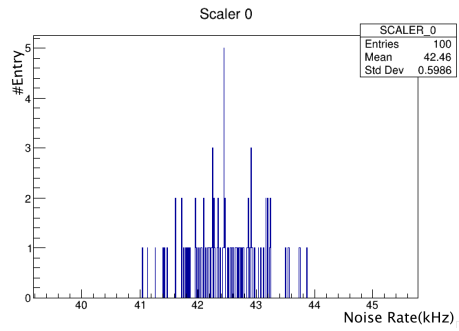
Figure 3.17: Noise rate distribution
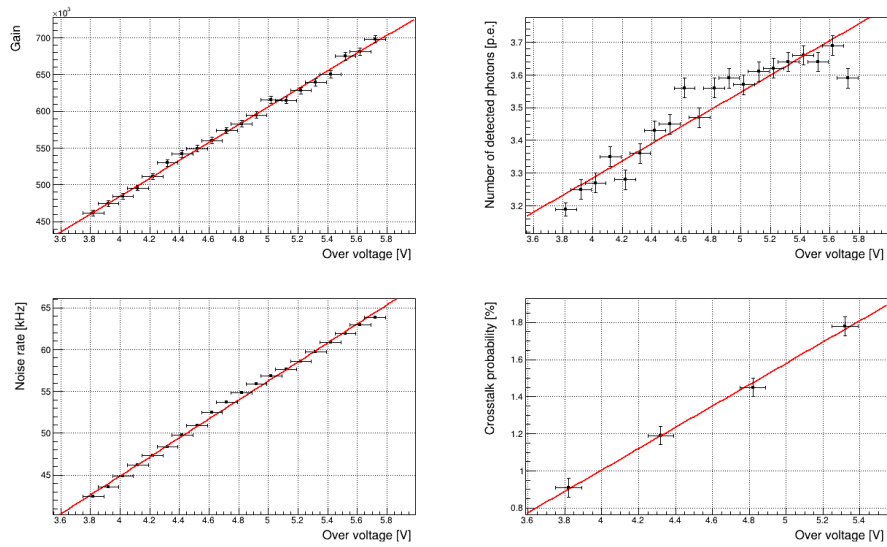
Figure 3.18: Summary of gain, number of the photon detected, noise rate and cross talk behavior under increasing over voltage

Chapter 4

Performance of the test system

As discussed in Table 3.1, the test system should meet certain requirements. This chapter discusses the development of five setups in the test system and their performances. Detailedly, this chapter presents temperature stability, background electromagnetic noise condition, consistency among multiple test sets, and cross-check between several setups.

4.1 Temperature stability

Many of the MPPC's characteristics have temperature dependencies. Thus, it is important to keep the temperature stable during the measurement. As discussed in previous chapters, we utilized two thermo-chambers in our test system. The new type MPPC-PCB has two temperature sensors, and we calibrated readings by the method discussed in Section 3.3.1. In this study, we checked the temperature stability, and the data being used are calibrated readings of MPPC-PCB sensors. Also, we want to see what is the preferred length of waiting time for the temperature to reach a stable level.

We first set the chamber temperature to 25°C and wait for enough time, so the initial condition of the temperature measuring is close to 25°C. Then we change the temperature setting to 20°C, which is the planned temperature used in the mass test, and record reading once every 10 seconds.

The temperature changing curve in Chamber 2 is shown in Figure 4.1, and the temperature changing curve in Chamber 1 with and without cover is shown in Figure 4.2. In general, then the temperature in chamber 2 is very stable after the temperature gets to a stable level. The temperature in Chamber 1 fluctuate periodically, but the amplitude of the fluctuation can be reduced by covering the MPPC-PCB with a black sheet. When without a black sheet cover, the temperature measured in chamber fluctuation width is about 1.3°C. The black cover sheet can reduce the fluctuation width to about 0.3 $^{\circ}$C, which should
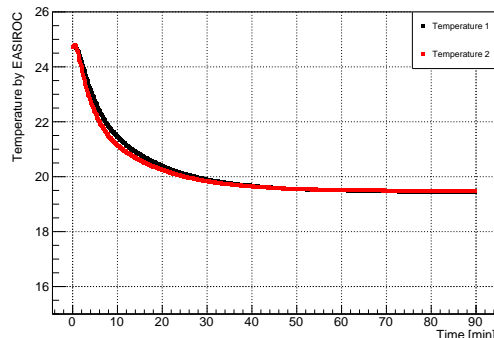
Figure 4.1: Temperature changing curve for Chamber2

be stable enough for the measurement purpose. A fluctuation within range of 0.5 °C should be enough, which corresponds to about 25mV difference in the breakdown voltage. Besides, the time required for the temperature to reach a stable level in Chamber 1 is longer with the cover is applied. After all, we decide that 40 minutes is a reasonable time duration for waiting for temperature stabilization before the main measurement.

4.2   Background electromagnetic noise condition

The background electromagnetic noise rate is measured when the bias voltage is 0 V, and the function generator sends a trigger while no light emitted. For the MPPC-PCBs in the test, the dark noise measurement is sensitive to background electromagnetic. Thus, it is crucial to keep the background electromagnetic noise at a low level. Compared to flat cables used for MPPC-PCBs, single lines used for reference MPPCs catch more noise. However, in case of reference MPPCs, measurements are only taken for ADC distribution for gain measurement. Thus, for reference MPPCs, we only check if ADC distributions of reference are clear enough for the peak finding.

We have accomplished suppressing noise for five setups. In the current condition, when chambers are in operation, setups with longer flat cables catch lots of noise. Figure 4.3 give the background noise condition used for eight setups by 8 test MPPC-PCBs when Chamber 1 and Chamber 2 are in operation. In general, the electromagnetic noise in setups 1, 2, 6, 7, 8 is low enough for the main measurement.
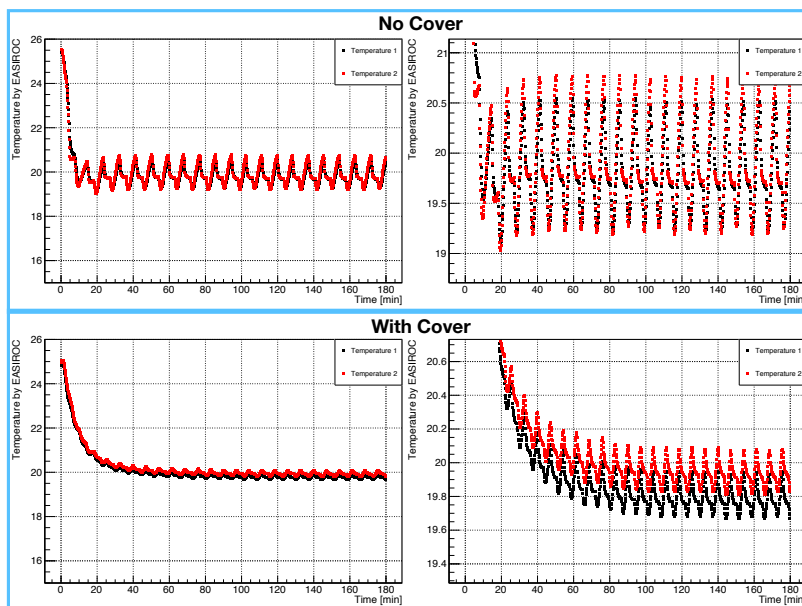
Figure 4.2: Temperature changing curve for Chamber1. Left: Temperature changing from 25°C to 20°C. Right: An enlarged temperature changing curve to show temperature fluctuation

4.3 Single setup consistency

Measurements results of one MPPC-PCB might differ from trial to trial. Thus, it is important to evaluate how stable results are. It is essential to check the single setup consistency of breakdown voltage because other interested values are recorded at a certain bias voltage which is based on the breakdown voltage. The fit of breakdown voltage is upstream of the whole analysis. Thus, we took five measurement trials with five setups in parallel operation and compared measured breakdown voltages.

We perform channel by channel measurement, as well as statistical results for each setup of five trials. All measurements are done at 20°C in two consecutive days with both chambers in operation. Measurements of five PCB are taken simultaneously by setup 1, setup 2, setup 6, setup 7 and setup 8, which have noises well-suppressed. In order to check the consistency of measurements, each setup takes measurements of the same PCB in five trials. Results of setup 1, setup 2, setup 6, setup 7 and setup 8 are shown in Figure 4.4, Figure 4.5, Figure 4.6, Figure 4.7 and Figure 4.8 correspondingly. Subplot(a)s show the channel by channel results measured in five trials; subplot(b)s show the histogram of breakdown voltages in each trial; subplot(c)s show the mean value change of five trails; subplot(d)s show the histogram of uncertainties of one

51
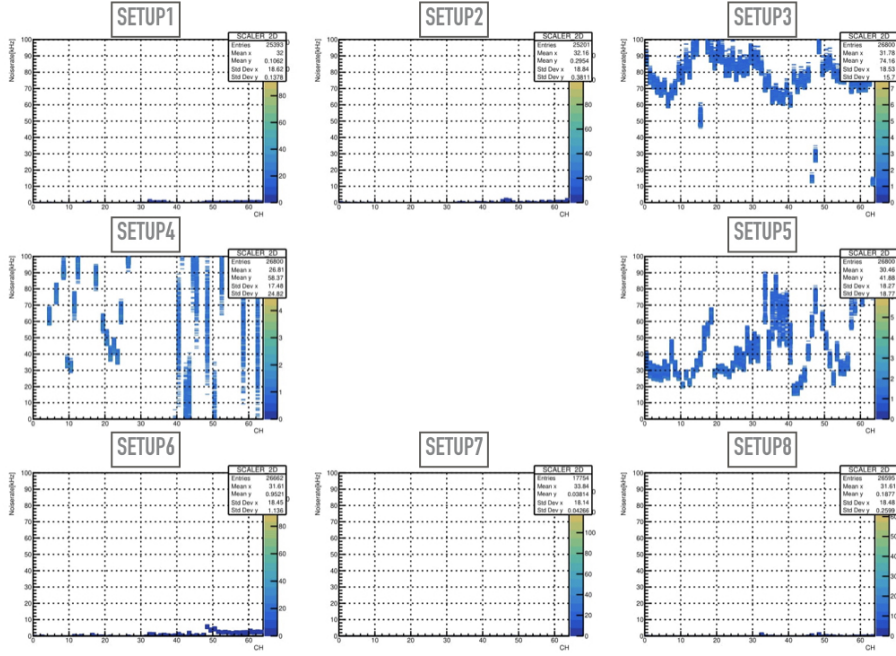
Figure 4.3: Background noise in operation

MPPC. A correlation of channel by channel performance between various trials can be seen for each setup. For setup 8, the mean uncertainty of the breakdown voltage measurements of one MPPC is 0.21 V, which is 0.16 V for setup 6 and setup 7 , 0.12 V for Setup 2, and 0.06 V for setup1. In general, the breakdown voltage measurement has larger uncertainty compared to operation voltage measurement due to the extrapolation process. 0.2 V is low enough for confirming that breakdown voltage variation is lower than $\pm$ 1.25V in one PCB board.

4.4 Setup cross check

We are expected to have multiple setups taking measurements of various PCBs in one trial. Thus it is important to understand the cross-setup consistency. Measurements of one PCB are done by setup 1 set 2, setup 7, and setup 8 independently. Setup 6 is not included in this study because it uses an old type interface board that will be replaced after another study is done. Results are shown in Figure 4.9.

In Figure 4.9, subplot(a) shows the channel by channel results measured in four setups; subplot(b) shows the histogram of breakdown voltages comparison
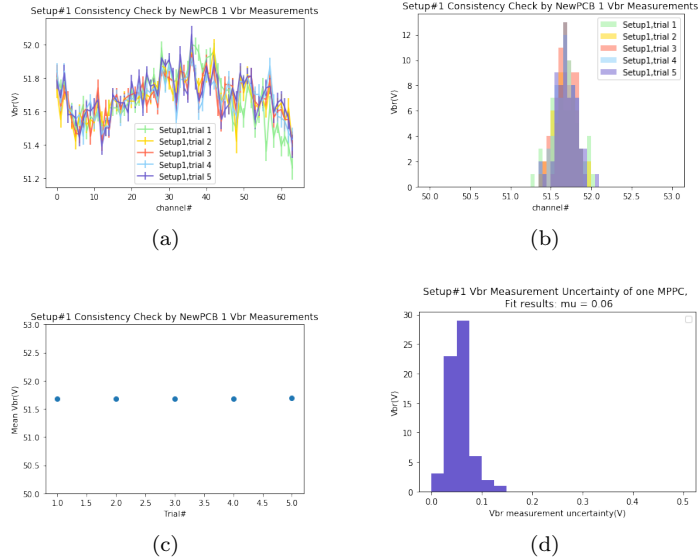
Figure 4.4: Setup1 consistency check by Vbr measurement (a): Channel by channel measurement; (b): Histograms of measured breakdown voltage; (c): Mean Breakdown Voltage in each Trial; (d):Histogram of measurement uncertainty of one MPPC.

in four setups; Subplot(c) shows the mean values of four setups; subplot(d) shows the histogram of cross-setup uncertainty of one MPPC. The channel by channel correlation between four setups is weak because of each setup's accumulated minor hardware difference. In general, the mean cross-setup uncertainty is 0.14 V, corresponds to 0.2% of the mean value. Thus, combining with the study in Section 4.3, the overall measurement uncertainty of breakdown voltage is 0.25V, corresponds to 0.65% of the mean breakdown voltage.

4.5   Measurements compared to Hamamatsu value

Hamamatsu provides their measurement of MPPC operation voltage before each delivery. They took measurements at $25°$C and defined the operation voltage as 5 V over breakdown voltage. In the mass test, we are planning to measure at 20 $°$C. Thus, to compare the Hamamatsu measured value, we take measurements at both 20 $°$and 25 degrees by the same setup in this study. Results are shown in Figure 4.10, Figure 4.12 and Figure 4.11.

Typically, the breakdown voltage differs by 50 mV per $°$C. Thus, the breakdown voltage is expected to vary by 250 mV at a five-degree difference. The mean voltage of the breakdown voltage measured by us is 51.53 V at $20°$C and
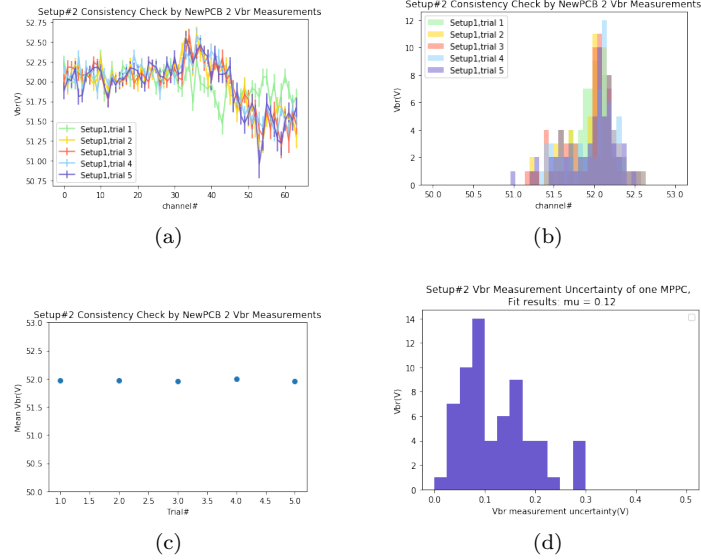
Figure 4.5: Setup2 consistency check by Vbr measurement (a): Channel by channel measurement; (b): Histograms of measured breakdown voltage; (c): Mean Breakdown Voltage in each trial; (d):Histogram of measurement uncertainty of one MPPC.

51.76V at 25°C, which differs by 230 mV and is consistent with expectation. It can also be confirmed by the peak around 0.25 V in Figure 4.12, which shows the distribution of the breakdown voltage difference between 25°C and 20°C. Hamamatsu mean value is 52.09 V at 25 °C. The difference between Utokyo measured value and Hamamatsu measured value is 0.33 V. This discrepancy can be explained by the reason that Hamamatsu is using current–voltage curve which is not the same as the direct measurement as we are doing. The discrepancy coming from the different methods is interpreted in [41]. The method of current–voltage curve is reported to give a larger breakdown voltage compared to the direct measurement. Also, the Utokyo measurement has a wider distribution compared to the Hamamatsu measurement. This wider distribution is a result of the extrapolation process of the breakdown voltage measurement.
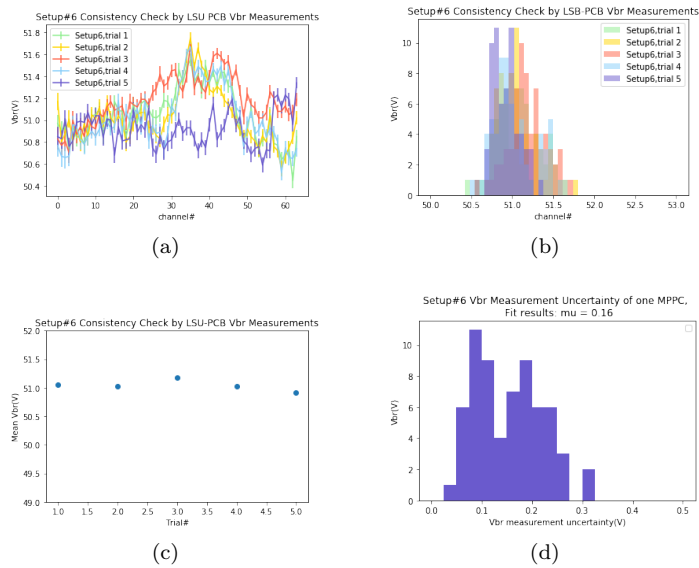
Figure 4.6: Setup6 consistency check by Vbr measurement (a): Channel by channel measurement; (b): Histograms of measured breakdown voltage; (c): Mean Breakdown Voltage in each trial; (d):Histogram of measurement uncertainty of one MPPC.
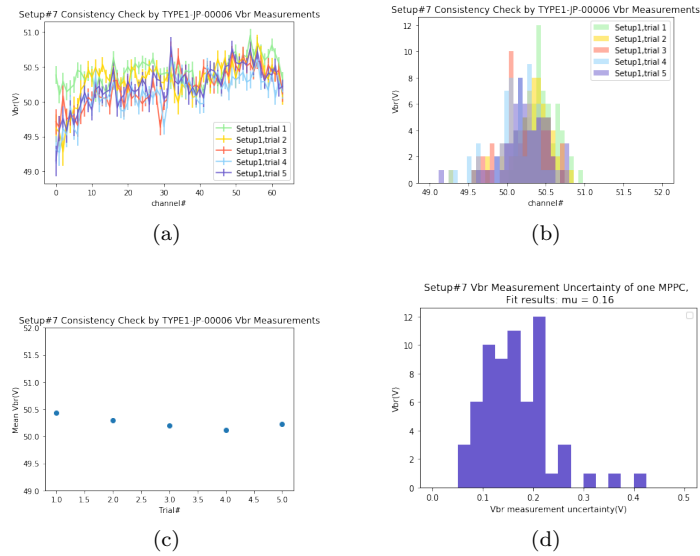
Figure 4.7: Setup7 consistency check by Vbr measurement (a): Channel by channel measurement; (b): Histograms of measured breakdown voltage; (c): Mean Breakdown Voltage in each trial; (d):Histogram of measurement uncertainty of one MPPC.

(a)   (b)

(c)   (d)
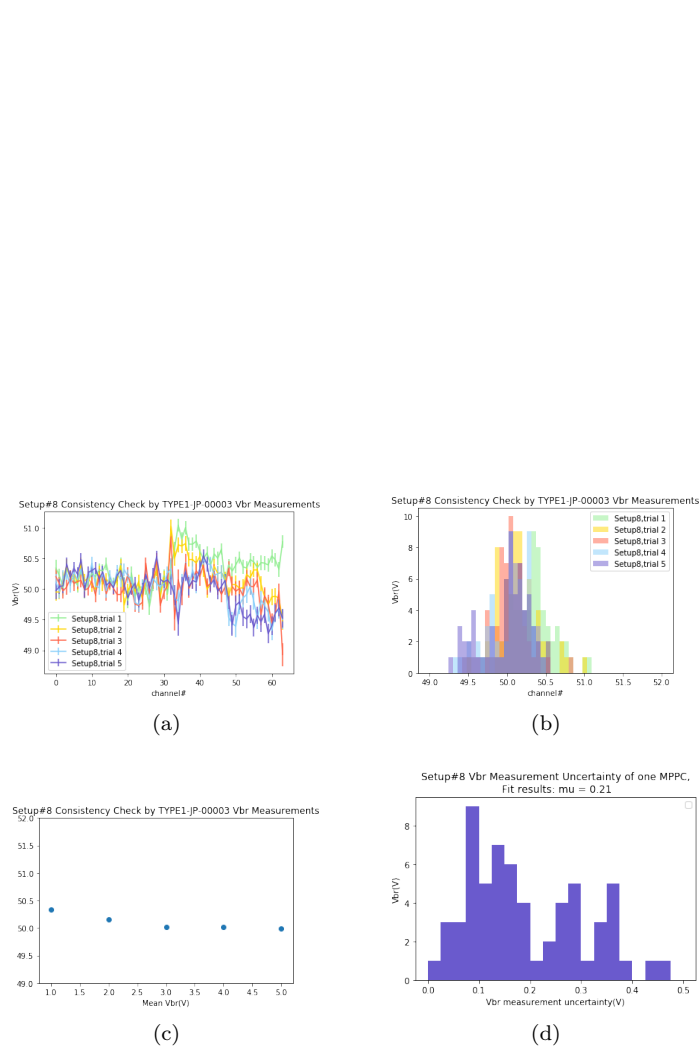
Figure 4.8: Setup8 consistency check by Vbr measurement (a): Channel by channel measurement; (b): Histograms of measured breakdown voltage; (c): Mean Breakdown Voltage in each trial; (d): Histogram of measurement uncertainty of one MPPC
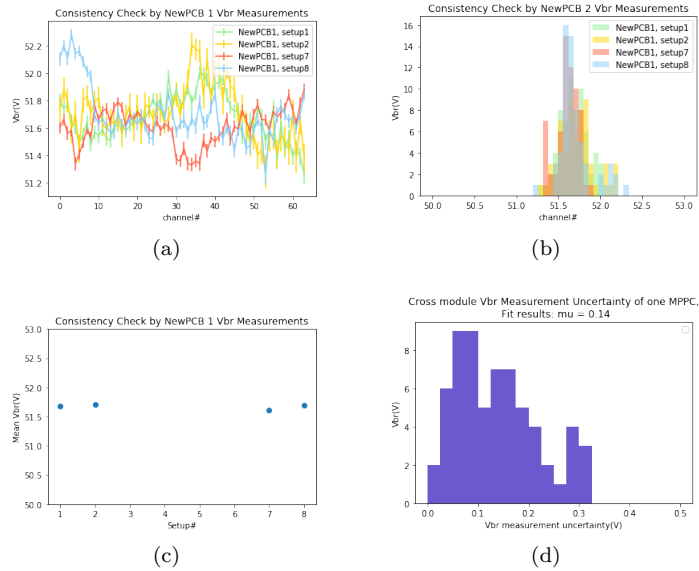
Figure 4.9: 4 Module consistency check by Vbr measurement (a): Channel by channel measurement; (b): Histograms of measured breakdown voltage; (c): Mean Breakdown Voltage in each module; (d): Histogram of measurement uncertainty of one MPPC cross module.
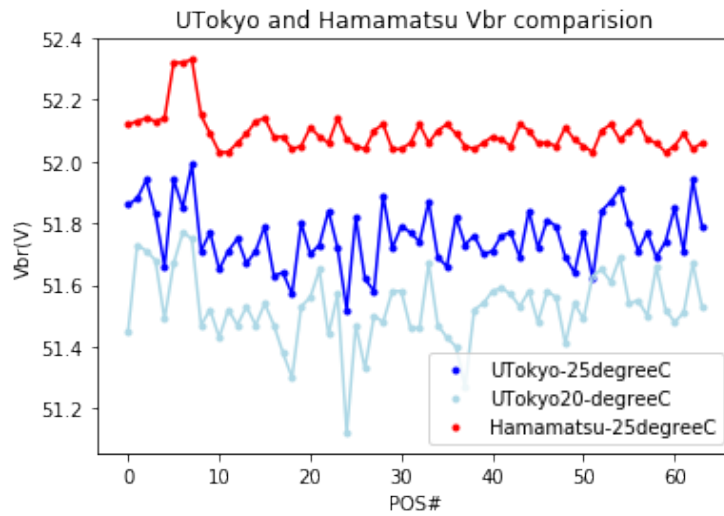
Figure 4.10: Utokyo measurement compared to Hamamatsu measurement: channel by channel comparison
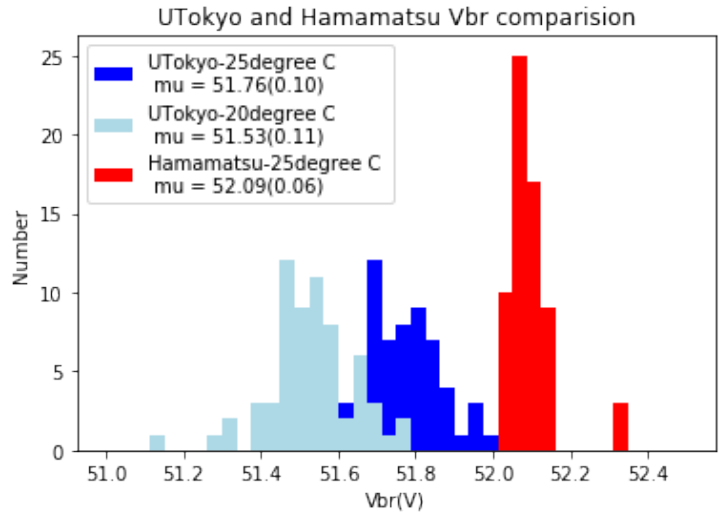
Figure 4.11: Utokyo measurement compared to Hamamatsu measurement: statistical comparison
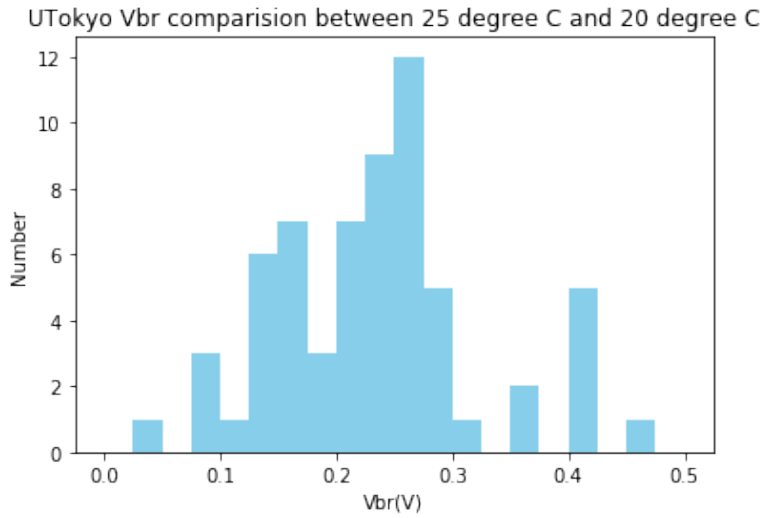
Figure 4.12: Difference between Utokyo Vbr at 25 degree C and 20 degree C

Chapter 5

Measurements of the first batch of MPPC-PCBs

The first batch of twelve MPPC-PCB boards arrives at the University of Tokyo in mid-June 2019. Six of the twelve PCBs are type one, and the other half are type two. Type one and type two are only different in the port's location on the board, as shown in Figure 5.1. MPPCs-PCBs are packed by bubble sheet packages and stored in the humidity monitoring box. During the measurement, we handle MPPC-PCBs with clean gloves. Figure 5.2 gives a photo of all first batch MPPC-PCBs. Measurements of the first batch MPPC-PCBs are important in confirming the quality of MPPCs before the mass production can finally start.

Measurements of twelve first batch MPPC-PCBs are done one by one and only by setup 7, which are stably free from the background electromagnetic noise, to reduce test system based uncertainty. In order for easy demonstration, type one PCBs are numbered as one to six and type two PCBs are numbered as seven to twelve in this chapter. The measurement procedure and analysis are the same as the designed procedure for the mass test as discussed in Subsection 3.3.2. The mass test is designed to be performed at a constant temperature 20°C; thus, we are presenting measurements taken under the same temperature in this chapter. Also, we calculate expected 25°C breakdown voltages in order to compare our breakdown voltage with Hamamatsu measured breakdown voltage.

5.1 Gain

Gains are reported at over-voltage 5 V as following in Figure 5.3. Gains are mostly in a range near $6{\times}10^5$ for all channels. The standard deviation of gains in all channels is $2.5{\times}10^4$, which is 4% of the mean value. The range of the gain is about ±12%, as shown in Figure 5.4. The detailed information of ADC distributions can be found in Appendix A.

(a)　　　　　　　　　　　　　　　　(b)

Figure 5.1: (a): Front side of two first batch MPPC-PCB (TYPE1 on the left; TYPE2 on the right) (b): Back side of two first batch MPPC-PCB (TYPE1 on the left; TYPE2 on the right)

5.2 Breakdown voltage

The breakdown voltage is calculated from the linear relationship between gain and bias voltages. Figure 5.5 gives a typical breakdown voltage fit in the first batch measurements.

Break down voltages are mostly around 50 V for all channels of the first batch MPPC-PCBs as shown in Figure B.6. The range of the breakdown voltage difference in each PCB is shown in Figure 5.7, which can be confirmed as all lower than 1.25 V. The detailed information of break down voltage distributions can be found in Appendix A.

5.2.1 Comparison between Hamamatsu measured value and Utokyo measured value

Hamamatsu measures operation voltage for each reel before delivery at 25 °C and defines the operation voltage as 5V over the breakdown voltage. Thus we can compare between the breakdown voltage distribution of the Hamamatsu measurement and the University of Tokyo measurement. Utokyo takes measurement at 20°C. Thus, we can covert 20°C value ($V_{br@20°C}$) to expected 25°C breakdown voltage ($V_{br@25°C}$) by

$$V_{br@25°C} = V_{br@20°C} + 0.25V. \tag{5.1}$$

This conversion is confirmed in Section 4.5. After all, results are shown in Figure 5.8.

The Utokyo measurement value has a lower mean value by 0.43V and larger distribution width, which is expected and explained in Section 4.5.

Figure 5.2: First batch of MPPC-PCBs

5.3 Dark noise rate

Dark noise rates are reported at over-voltage 5V as following in Figure 5.9. Means of dark rates of all MPPC-PCBs are in the range of 20 to 25 kHz and the distribution standard deviation is about 5kHz. The detailed information of dark noise rate distributions can be found in Appendix A.

5.4 Cross talk

Cross talk are reported for over-voltage 5V as shown in Figure 5.10. Mean cross-talk is lower than 1.5% for all MPPC-PCBs. The distribution width of the cross talk is within 0.5%. The detailed information of cross-talk probability distributions can be found in Appendix A.

5.5 Relative PDE

Relative PDE are reported for over-voltage 5V as shown in Figure 5.11 and Figure 5.12. Mean relative PDE is about 1.2. The standard deviation of all MPPCs in the first batch is 0.04, which is 3.2% of the mean. The range of the distribution is $\pm$ 12%. The detailed information of relative PDE distributions can be found in Appendix A.

5.6 Summary

In general, the measurement results of the first batch of MPPC-PCBs can be concluded in Table 5.1.
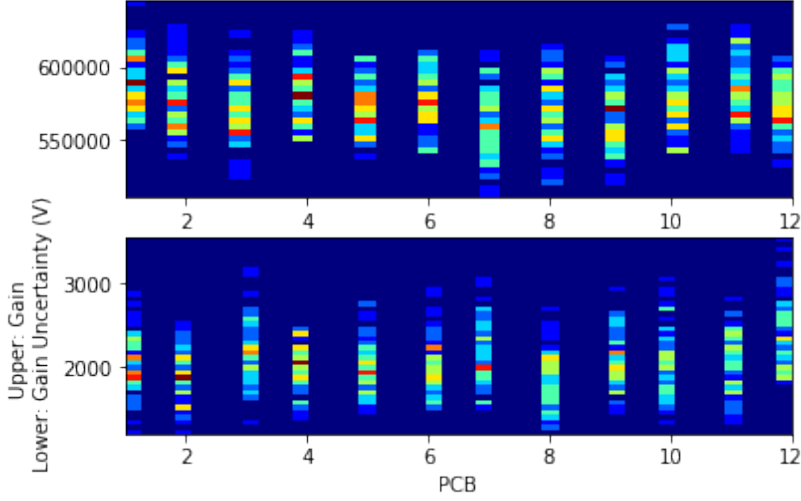
Figure 5.3: Gain of the first batch MPPC-PCBs at 20 $^{\circ}$C

Table 5.1: Characteristics of the First batch MPPC at 20 $^{\circ}$C

Item	Characteristics
Gain	range = ± 12%
Breakdown voltage	range ≤ 1.5 V in each PCB
Dark Noise rate	≤ 40kHz
Crosstalk probability	2%
Relative PDE	range = ±12%

Compared to the MPPC requirement for the SuperFGD discussed in Table 2.2, it is safe to conclude that the first batch of MPPC-PCB fulfils requirements on gain, breakdown voltage, dark noise rate, crosstalk probability for SuperFGD. The relative PDE is slightly larger than the requirement, but if looking to Figure 5.11, for each measurement the distribution is about same width but the mean value fluctuate, so it is might be caused by reference MPPC measurement instability, and the actual range of relative PDE is actually lower.
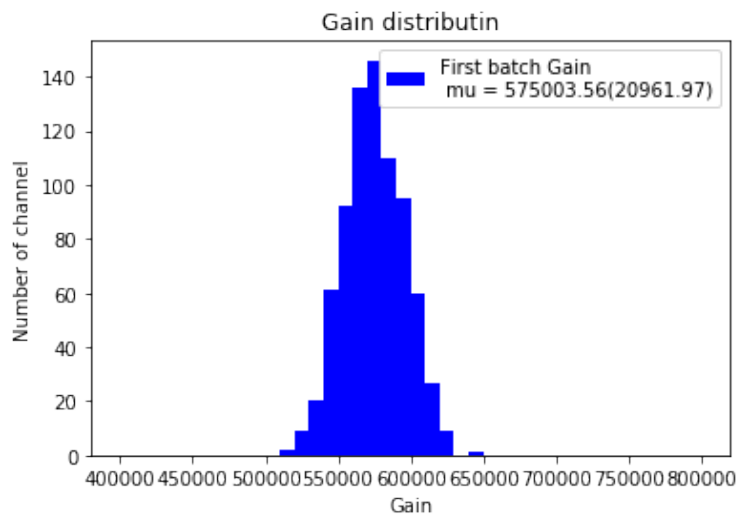
Figure 5.4: Gain range of the first batch MPPC-PCBs at 20 °C
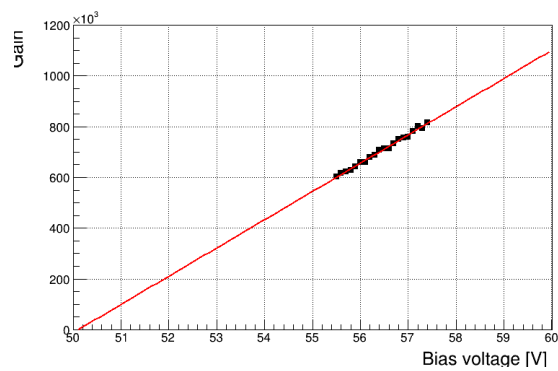
Figure 5.5: A typical break down voltage fit(TYPE2-JP-00001(No.7), channel 6)
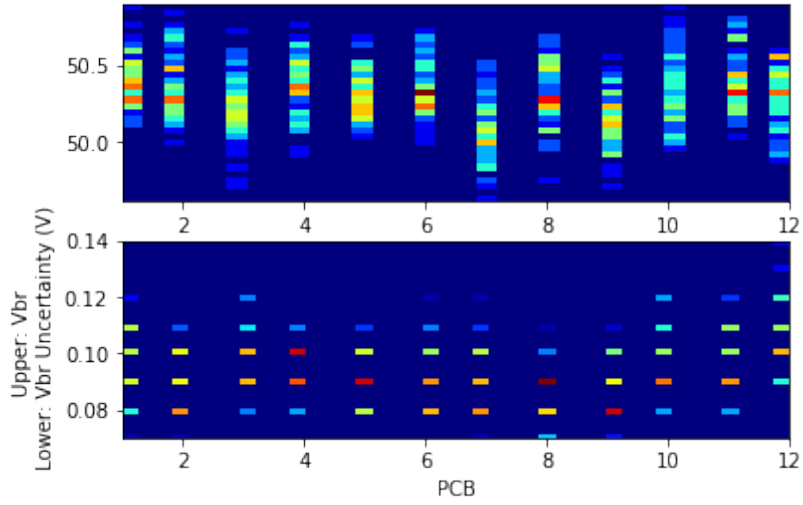
Figure 5.6: Breakdown voltage of the first batch MPPC-PCBs at 20 °C
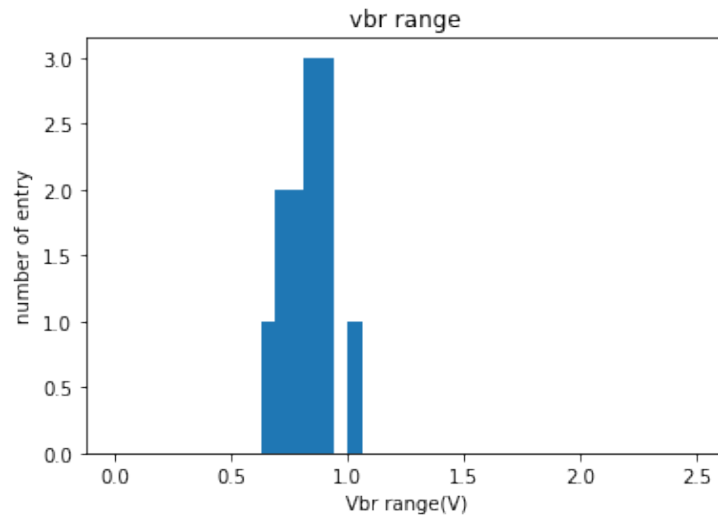
Figure 5.7: Breakdown voltage range of the first batch MPPC-PCBs at 20 °C

65
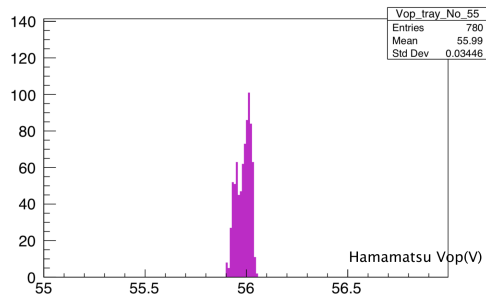
(a)
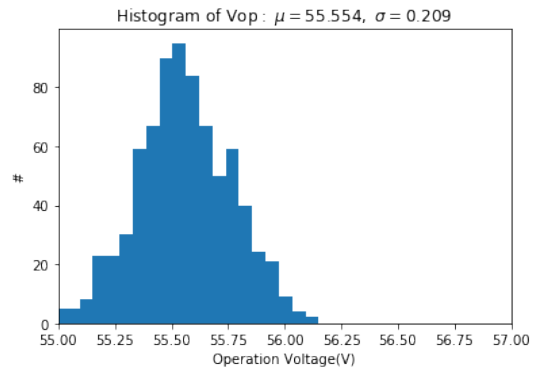
(b)

Figure 5.8: (a): Hamamatsu measured Vop of the MPPC used in the first batch; (b): Utokyo measured Vop of the first batch
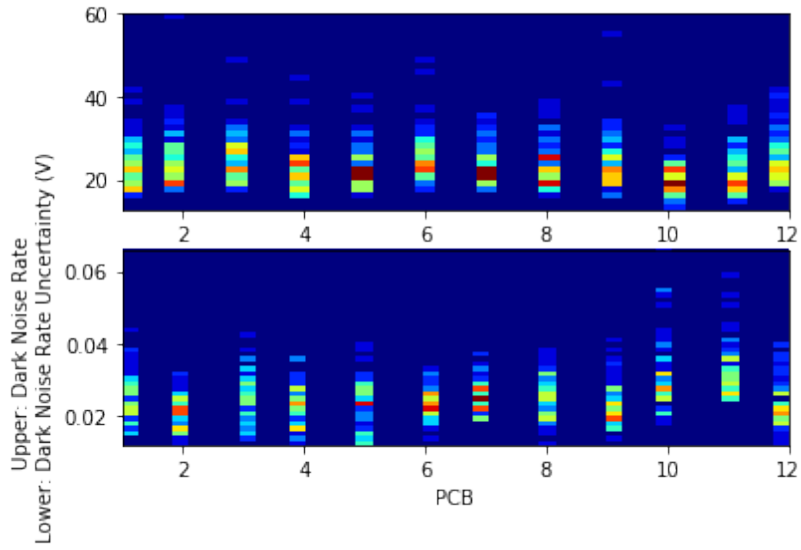
Figure 5.9: Dark Noise Rate of the first batch MPPC-PCBs at 20 °C
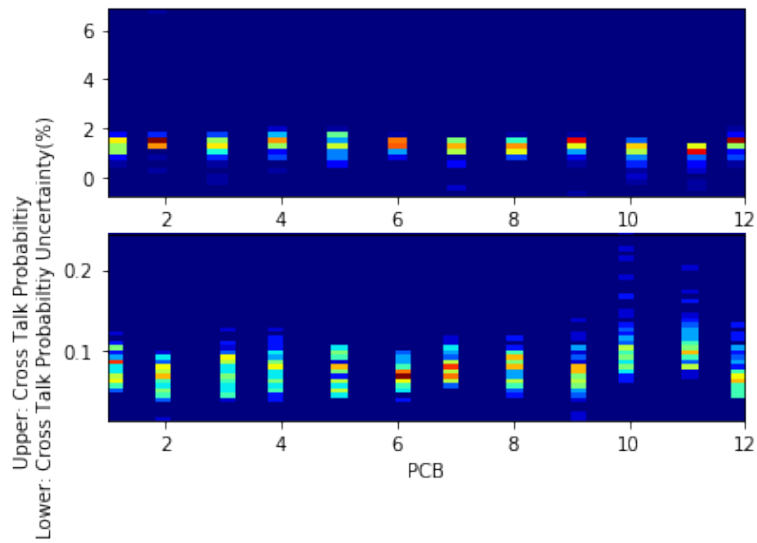
Figure 5.10: Cross Talk of the first batch of Type 2 MPPC-PCBs at 20 °C
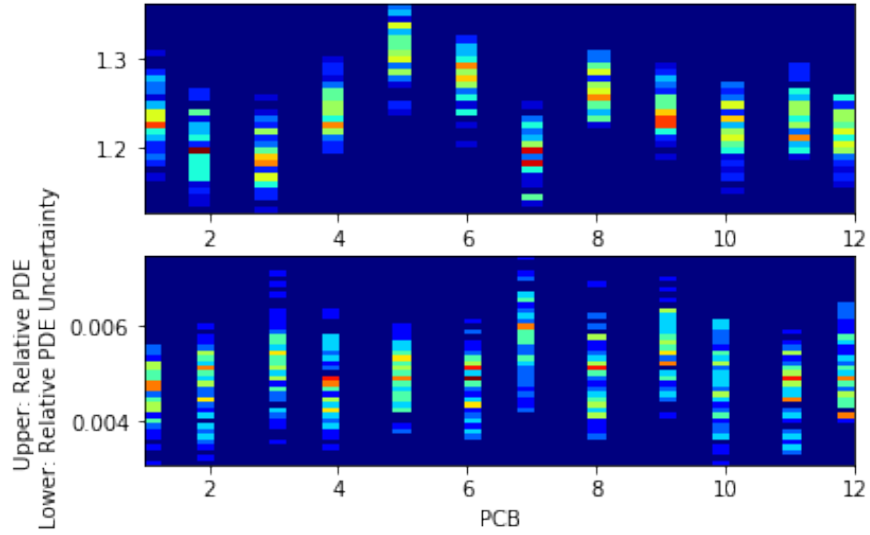
Figure 5.11: Relative PDE of the first batch MPPC-PCBs at 20 °C
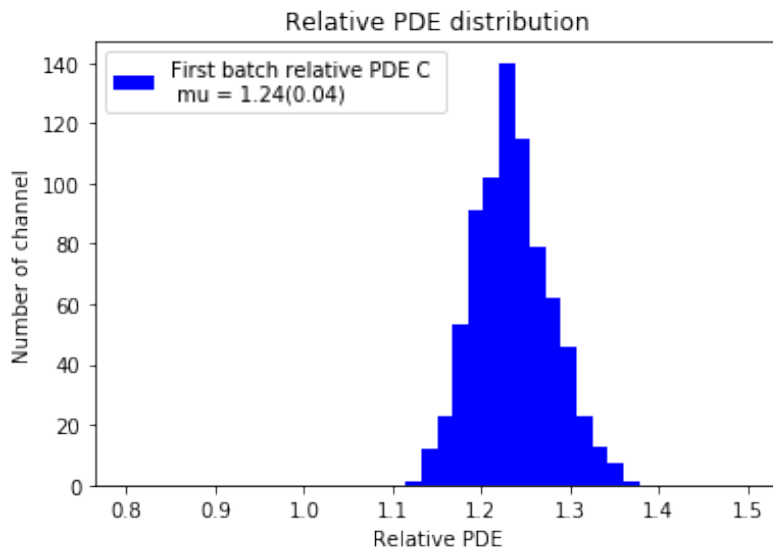
Figure 5.12: Histogram of relative PDE of all first batch MPPCs at 20 °C

Chapter 6

Future prospects

6.1 Things to be done

The development of the MPPC-PCB test system has not been completed yet. There still left lots of tasks to be complete.

6.1.1 Temperature monitoring

As discussed, we are able to record the PCB board temperature by reading from temperature sensors, but it is relatively hard to record the temperature change all over the main test by reading from temperature sensors on the PCB board. Thus, we are planning to utilize a new external temperature monitoring device to monitor the temperature change in chambers over the whole measurement procedure.

6.1.2 Data management system and registration system

The data management system is not completed now. We must consider the value to be registered to the data management system. Also, we want to integrate an easier way to initialize each testing trial and register results.

6.1.3 Light source check

Eight light sources should be checked in order to finalize the relative photon detection efficiency measurement.

6.1.4 Comparison between US group

We are still unsure of the cause of the breakdown voltage measurement between the Japan and US groups. We exchange rare data in order to understand the difference. We also need to compare gain, noise rate, and cross talk after

comparing the breakdown voltage. The current progress is discussed in Figure B.3.

6.1.5 Setup improvement

Now setup1 has a good stability for measurements, we will improve the stability of other setups. Also, we will try to improve cross-setup the channel by channel performance by adjusting adjustable voltage in each module.

6.1.6 Expansion to eight test setups

We plan to make use of eight modules in total. However, there are three setups now correctly suffering form background noise problem. Background electromagnetic noise is a critical issue for some of the setups, noise of which is too large for precise dark noise measurement. Thus, we must figure out a better arrangement for the test setups to suppress background noise to a stable level for all setups. We will try to suppress noise for this three setups. Thus the whole measurement period can be shorten to one month.

Chapter 7

Summary

T2K collaboration is working on the ND280 upgrade to reduce neutrino interaction model base systematic uncertainty in the neutrino oscillation experiment. Among upgrade detectors, SuperFGD is a scintillator target detector which enables three dimensional readouts. It is expected to provide effective particle tracking at all polar angles.

It is necessary to confirm that 56,384 MPPCs, which are used as photonsensors in SuperFGD, behaves as expected and meet certain requirements before being installed. The future mass test will check gain, dark noise rate, breakdown voltage, relative photon detection efficiency and cross talk probability for each MPPCs. Thus, we develop a test system which enables five measurements simultaneously in one trial.

The first batch of the produced MPPC-PCBs has been checked. From the measurement results, we can conclude that the first batch of MPPC-PCBs is meeting the requirements of breakdown voltage, dark noise rate and gain.

Appendix A

Detailed measurement results of the first batch MPPC-PCBs

As discussed in Chapter 5, we measure the gain, break down voltage, cross talk and dark noise rate of the first batch of the type one and type 2 MPPC-PCBS. Gain, cross talk and dark noise rate are reported at over voltage 5V. Distributions of each PCB are shown as following. Type one MPPC-PCBs are labelled as No.1 to No.6 and Type two MPPC-PCBs are labelled are No.7 to No.12 correspondingly.
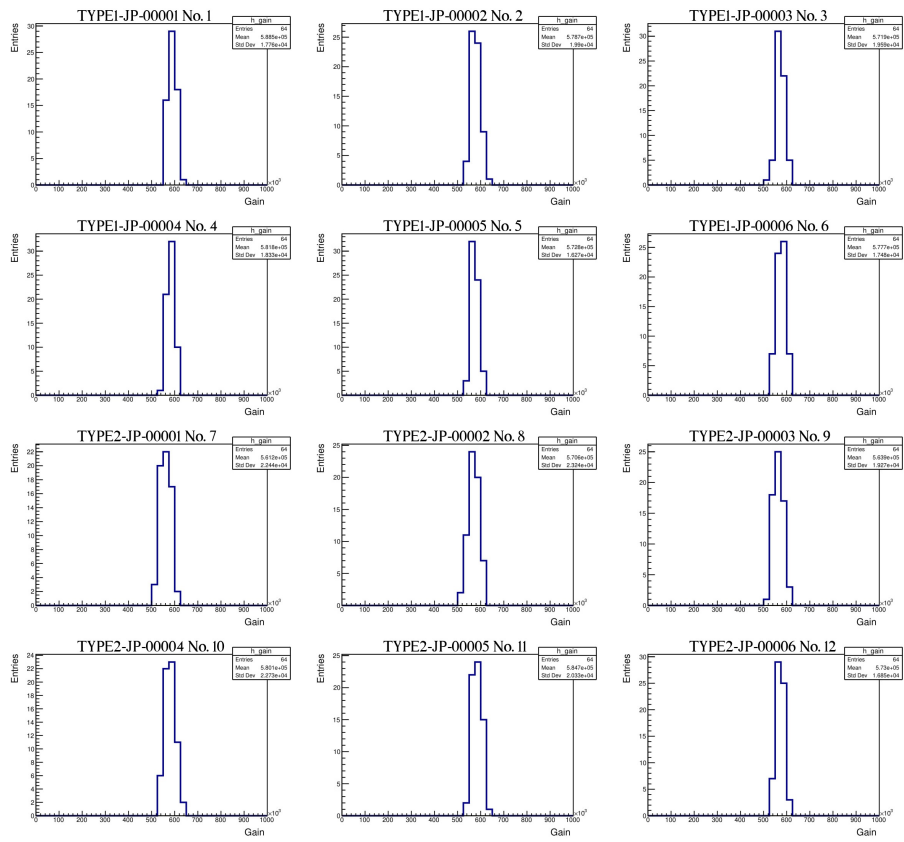
Figure A.1: Gain of the first batch MPPC-PCBs at 20 °C at over voltage =5V
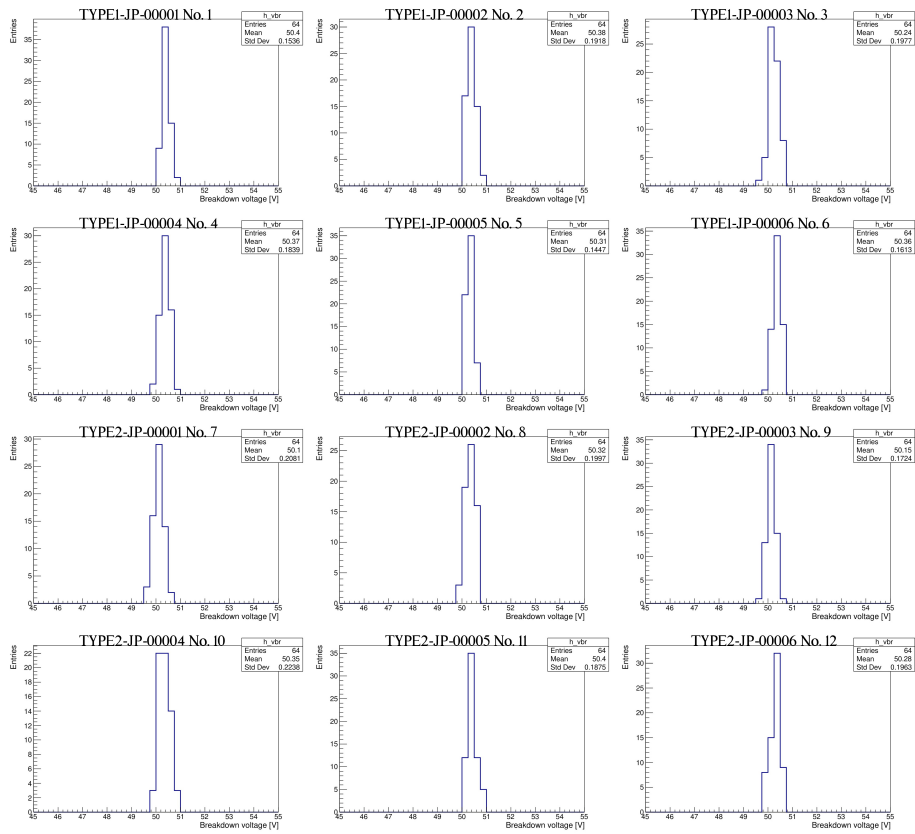
Figure A.2: Breakdown voltage of the first batch MPPC-PCBs at 20 °C
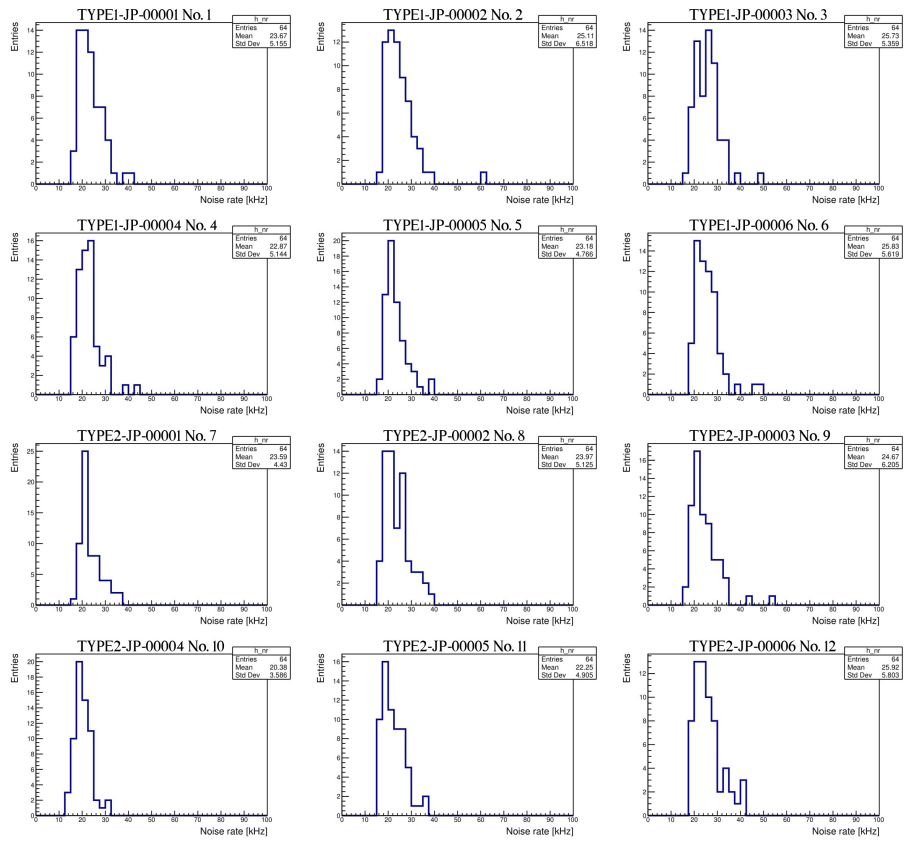
Figure A.3: Dark Noise Rate of the first batch MPPC-PCBs at 20 °C at over voltage =5V
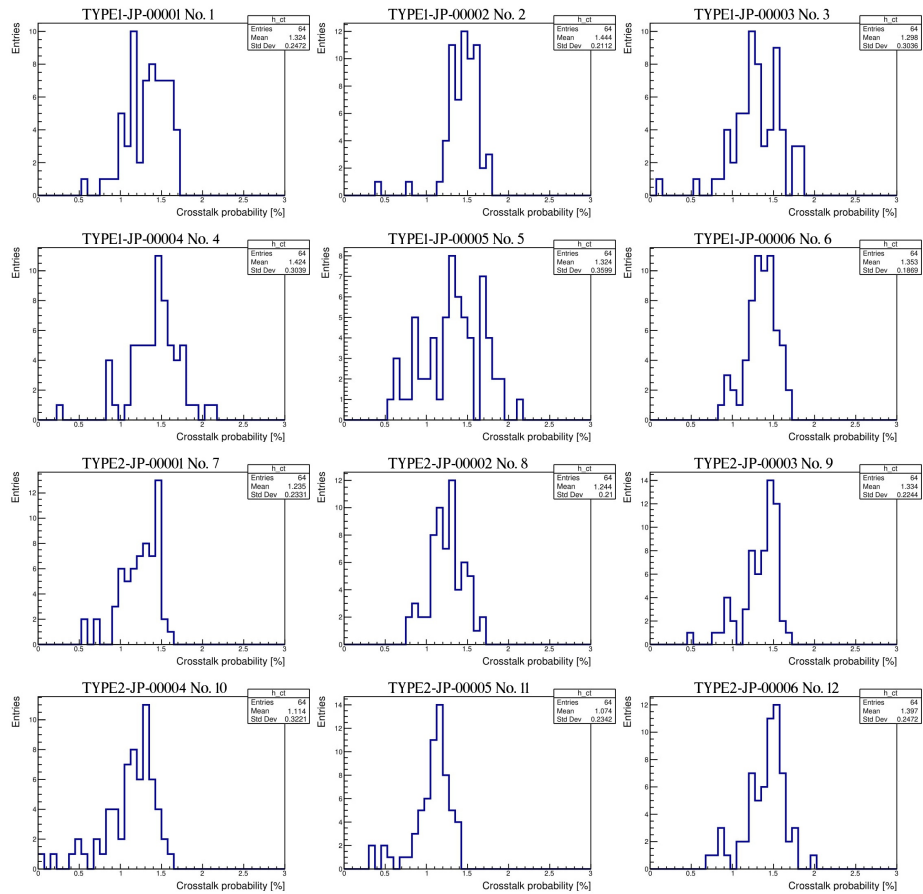
Figure A.4: Cross Talk of the first batch of Type 2 MPPC-PCBs at 20 °C at over voltage =5V
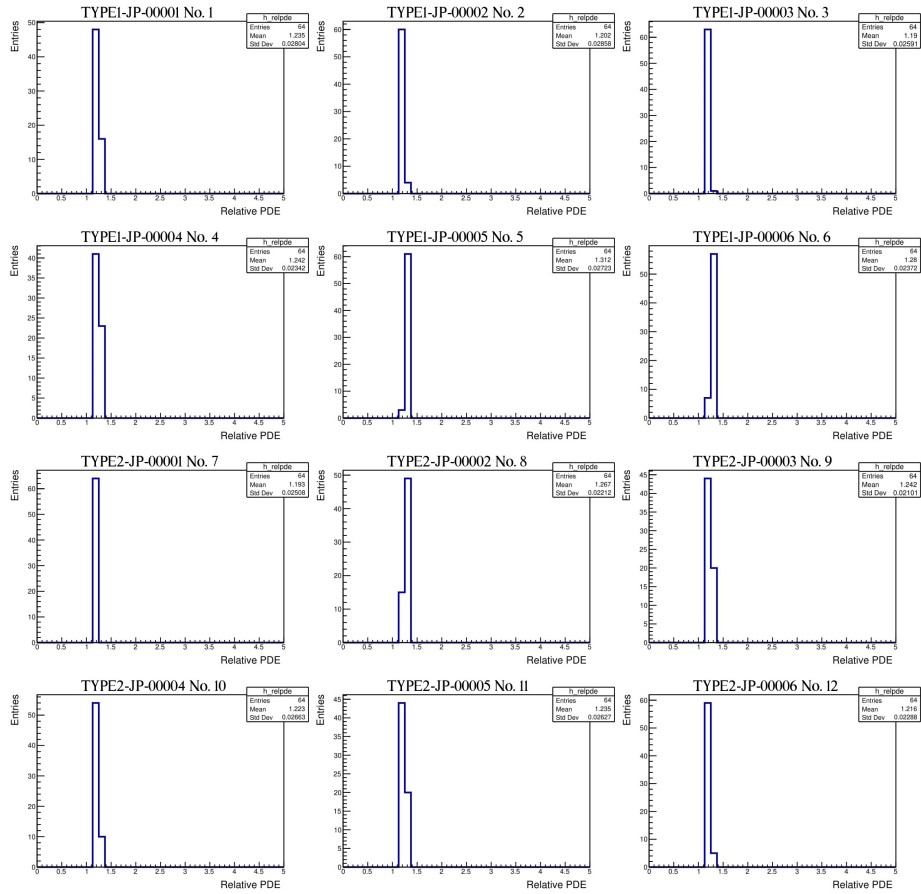
Figure A.5: Relative PDE of the first batch of Type 2 MPPC-PCBs at 20 °C at over voltage =5V

Appendix B

Cross-check with US group measurement

There will be about 10k MPPCs in the United States tested by a working group in Louisiana State University. Thus, it is important to compare the measurement and analysis results between the US group and us to understand the discrepancy. In order to do so, we exchanged two MPPC-PCB boards in May 2021 and are driving to some primary results.

B.1   US test system and analysis procedure

A schematic view of the US setup is shown in Figure B.1[42]. They use two CAEN DT5702 as the MPPC readout board for each MPPC-PCB. Each of the boards contains 32 channels. Agilent 6700B is used to provide power for the test system, and the Thermo Scientific NESLAB RTE 10 Bath is used to keep a stable ambient temperature during the measurement.

The methodology of data processing is similar to ours but differs in details. The US group determine the gain at a certain bias voltage by fitting the ADC spectrum peak positions to the PE number by a linear relation, which is shown in B.2a. The breakdown voltage is that decided by linearly fitting the gain and the bias voltage as shown in B.2b.

B.2   US-produced MPPC-PCB

In order for measurement comparison, we took several measurements of exchanged US-produced PCB. Peaks of ADC distributions of the US-PCB is blurred when given stronger light. B.3a shows a typical ADC distribution at lower luminosity, and B.3b gives an ADC distribution of the same channel when luminosity gets higher.
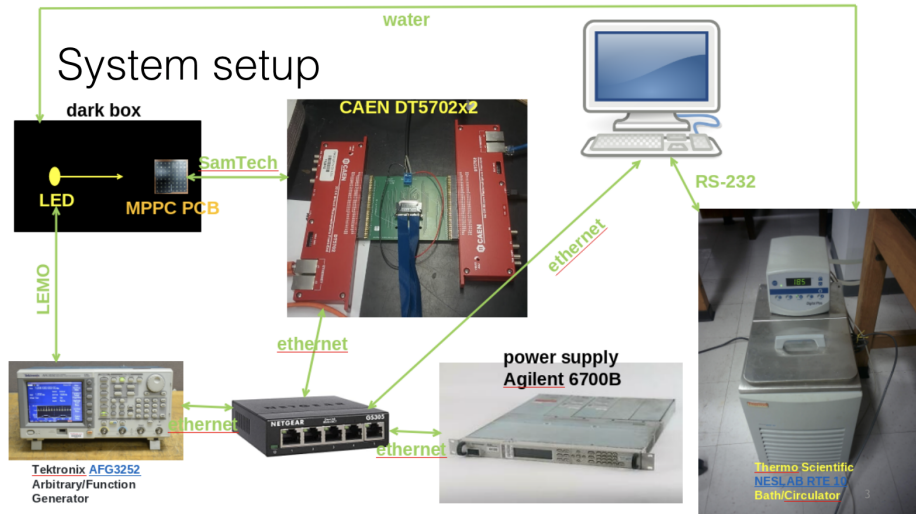
Figure B.1: US MPPC setup

The calculation of the gain from peak finding is in the very early stage of the whole analysis. We study noise rate, cross talk and the number of detected photons at over-voltage equal five voltage, which is chosen on the base of the break down voltage fitted from the relationship of gain and bias voltage. Thus, it is important to evaluate how this blurred peak will affect the result. We compare the values between measurements taken at a fixed bias voltage 57V and the fitted value at over-voltage 5 V from the analysis process.

Figure B.4 plots the gain as the luminosity changed. The luminosity cannot be quantified by the light source. Thus we use the number of the detected photon electron as an alternative demonstration of the light strength. The upper right graph shows the gain at a fixed bias voltage. It can be clearly seen that when the number of the photon electron increase, the measurement uncertainty of the gain increase.

Figure B.5 gives a relationship between the fitted value of the breakdown voltage and the number of detected photon electron. As the luminosity gets higher, the fitted breakdown voltage gets lower, and the uncertainty rises up. Thus, the gain measured at over-voltage 5 V also catches this tendency which can be seen in the upper-left subplot of Figure B.5. The uncertainty of the number of photon electron measurement also increases as shown in the lower-left subplot of Figure B.5.

The dark noise rate and cross talk are measured while the LED is turned off. Thus they should intrinsically not be influenced by the luminosity setting of the testing trial, as shown in the upper and lower right subplots in the Figure B.6. However, when fitting for the noise rate and cross talk at the 5 V over-voltage,
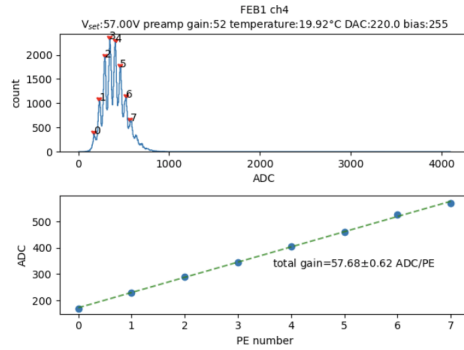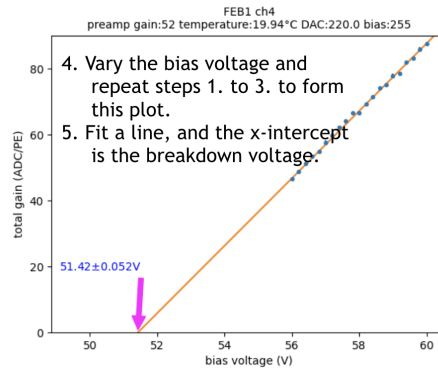
Figure B.2: (a): finger plot ;(b): vbr fit

they catch the same tendency and the uncertainty arising from the breakdown voltage. Thus, in the upper and lower left subplot of Figure B.6, dark noise rate and cross talk measured at 5V overvoltage slightly goes down, and their uncertainty rise up when luminosity gets higher, although they should not be directly influenced by the luminosity.

B.3   Measurement comparison

The measurement of the breakdown voltage is upstream of the whole analysis process. Thus, understanding the comparison between the Japan side measurement of breakdown voltage and the US side measurement is important. This study is done by comparing the measurements of the same PCB board by both the Japan group and the US group. Figure B.7 gives a comparison between the Japan measured breakdown voltage and gain at an over-voltage of 5 volts
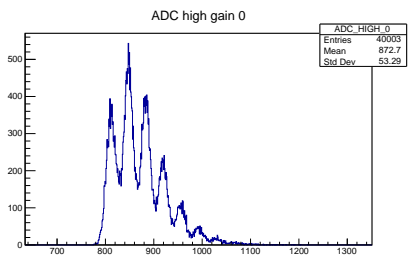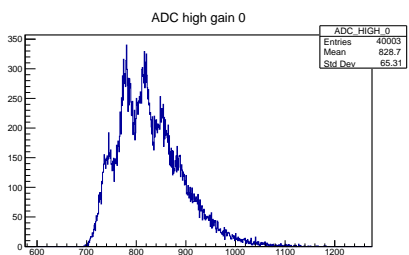
Figure B.3: (a): A good ADC distribution ;(b):A blurred ADC distribution

and the US measured value for the exchanged PCB produced in the US. The measurements are taken both at 20°C and 25°C. In this study, the data set taken at lower luminosity which gives a better peak resolution, is chosen.

The US side measurement is marked as "LSU", and the Japan side measurement is marked as "UTokyo". It is clear that the UTokyo measured breakdown voltage is lower than the LSU value by about 1 volt, and LSU measurement is catching more outliers compared to the Utokyo measurement. Also, the correlation between the two measurements seems to be weak. The discrepancy of breakdown voltage can come from both hardware and analysis method. The discrepancy of gain at over-voltage equals five voltage can be raised from the difference of the breakdown voltage. Thus, understanding the breakdown voltage discrepancy is the primary goal. We are now collaborating with the US group in order to understand the discrepancy.
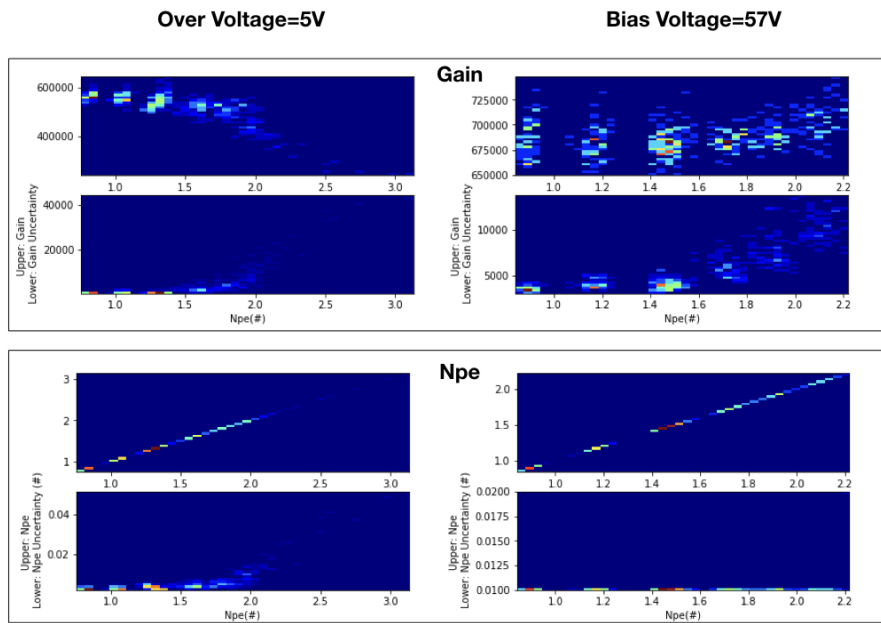
Figure B.4: Gain and Number of detected Photon of US-produced PCB (Left: Fitted value at over voltage=5V; Right: Measured value at Bias voltage=57V)
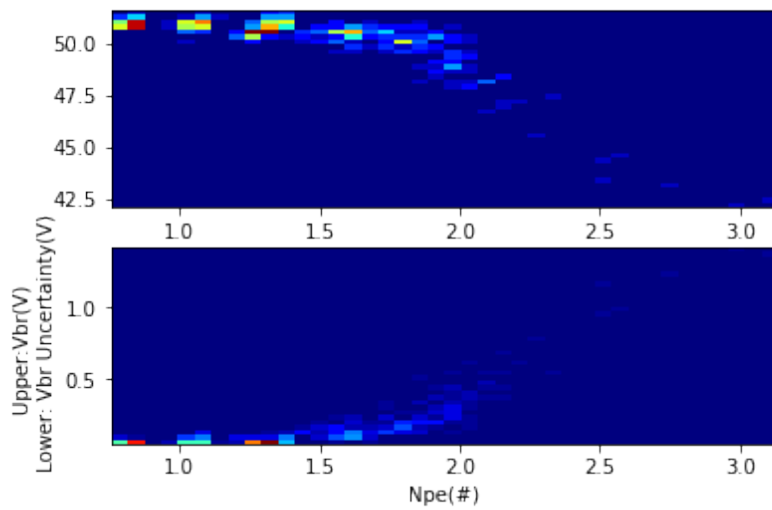
Figure B.5: Break Down Voltage vs luminosity (number of detected photon electron) of US-produced PCB (Left: Break Down Voltage fit for over voltage=5V; Right: Break Down Voltage measured at Bias voltage=57V)
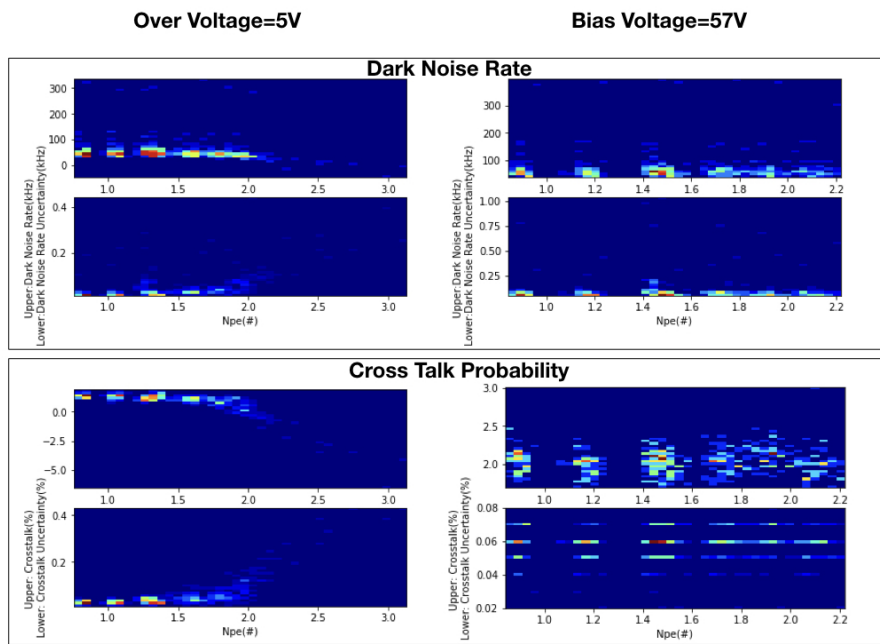
Figure B.6: Noise rate and cross talk of detected Photon of US-produced PCB(Left: Fitted value at over voltage=5V; Right: Measured value at Bias voltage=57V)
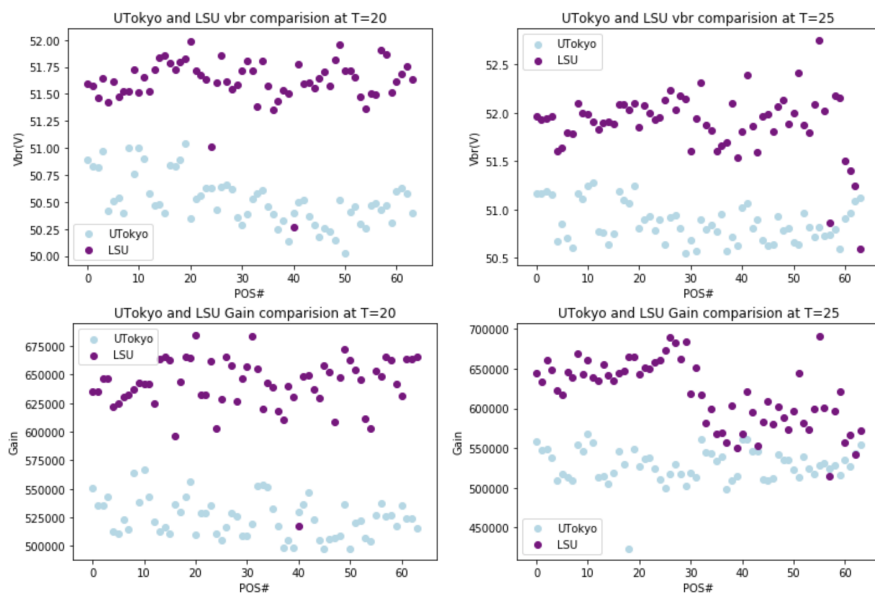
Figure B.7: Comparison between Japan and US group:Upper: breakdown voltage; Lower: Gain at over voltage = 5 volt

List of Figures

List of Tables

Bibliography

[1] Mark Thomson. *Modern Particle Physics*. Cambridge University Press; 1st edition, 2013.

[2] B Pontecorvo. "Mesonium and anti-mesonium". In: *Sov.Phys.JETP* 6 (1957), p. 429.

[3] B Pontecorvo. "Neutrino Experiments and the Problem of Conservation of Leptonic Charge". In: *Sov.Phys.JETP* 26 (1968), pp. 984–988.

[4] Z. Maki; M. Nakagawa; S. Sakata. "Remarks on the Unified Model of Elementary Particles". In: *Prog.Theor.Phys* 28 (1962), pp. 870–880.

[5] Boris Kayser. "Neutrino Physics". In: *eConf C040802* L004 (2004). eprint: `arXiv:hep-ph/0506165`.

[6] Wai-Yee Keung(Brookhaven) Ling-Lie Chau(Brookhaven). "Comments on the Parametrization of the Kobayashi-Maskawa Matrix". In: *PhysRevLett* 53.1802 (1984).

[7] Carlo Giunti and Chung W.Kim. *Neutrino Physics and Astrophysics*. Oxford University Press, 2007.

[8] Thomas Mannel. "Theory and Phenomenology of CP Violation". In: *Nuclear Physics B.* 167 (2006).

[9] Alexandre Sousa. "Long-Baseline Neutrino Oscillation Experiments". In: (2011). eprint: `arXiv:1102.1125`.

[10] S. Gariazzo et al. "Neutrino masses and their ordering: Global Data, Priors and Models". In: (2018). DOI: `10.1088/1475-7516/2018/03/011`. eprint: `arXiv:1801.04946`.

[11] T2K Collaboration. "Measurement of the CCQE cross section on carbon with the ND280 detector at T2K". In: (2014). DOI: `10.1103/PhysRevD.92.112003`. eprint: `arXiv:1411.6264`.

[12] J. Nieves, I. Ruiz Simo, and M. J. Vicente Vacas. "Inclusive Charged–Current Neutrino–Nucleus Reactions". In: (2011). DOI: `10.1103/PhysRevC.83.045501`. eprint: `arXiv:1102.2777`.

[13] R. Gran et al. "Neutrino-nucleus quasi-elastic and 2p2h interactions up to 10 GeV". In: (2013). DOI: `10.1103/PhysRevD.88.113007`. eprint: `arXiv:1307.8105`.

[14] Juan Nieves. "2p2h Excitations, MEC, Nucleon Correlations and Other Sources of QE-like Events". In: *JPS Conf. Proc.* 11 (2016).

[15] T2k Collaboration. URL: t2k-experiment.org/t2k/.

[16] T2K Collaboration. "Improved constraints on neutrino mixing from the T2K experiment with $\mathbf{3.13 \times 10^{21}}$ protons on target". In: (2021). arXiv: 2101.03779.

[17] T2K Collaboration. "The T2K Neutrino Flux Prediction". In: (2012). DOI: 10.1103/PhysRevD.87.012001. arXiv: 1211.0469.

[18] T2K Collaboration and J-PARC Neutrino Facility Group. "J-PARC Neutrino Beamline Upgrade Technical Design Report". In: (2019). eprint: arXiv:1908.05141.

[19] T2K Collaboration. "Measurement of neutrino and antineutrino oscillations by the T2K experiment including a new additional sample of $_e$ interactions at the far detector". In: (2017). DOI: 10.1103/PhysRevD.96.092006. arXiv: 1707.01048.

[20] T2K Collaboration. "The T2K Experiment". In: (2011). DOI: 10.1016/j.nima.2011.06.067. arXiv: 1106.1238.

[21] M. Antonova. "Baby MIND: A magnetised spectrometer for the WAGASCI experiment". In: (2017). arXiv: 1704.08079.

[22] Kamioka Observatory. URL: http://www-sk.icrr.u-tokyo.ac.jp/sk/tankopen2018/photo-e.html.

[23] The T2K ND280 Upgrade Working Group. "The T2K-ND280 upgrade proposal". In: (2017).

[24] K.Ieki. "Observation of $\nu_\mu \to \nu_e$ oscillation in the T2K experiment". PhD thesis. Kyoto University, Japan, 2014.

[25] K. Abe et al. "T2K ND280 Upgrade – Technical Design Report". In: (2019). arXiv: 1901.03750.

[26] H. Kikutani. "Development of performance test system of mass-produced Multi-Pixel Photon Counters for a new neutrino detector". MA thesis. University of Tokyo, 2020.

[27] Koei Yamamoto. "Recent Development of MPPC at Hamamatsu for Photon Counting Applications". In: *JPS Conf.Proc.* 27 (2019).

[28] Hamamatsu Photonics K.K. *S13360series, MPPCs for precision measurement.*

[29] Tsunayuki Matsubara for the T2K ND280 upgrade group. "Application of MPPC for T2K near Detector Upgrade". In: *JPS Conf. Proc.* 27 (2019).

[30] Hamamatsu Photonics K.K. *Handbook Introduction.*

[31] D.Renker. "Geiger-mode avalanche photodiodes, history, properties and problems". In: *Nucl.Instrum.Meth.A* 567 (2006), pp. 48–56.

[32] SIBYLLE I. ZIEGLER BERND J. PICHLER. *Emission Tomography*. 2004.

[33] Hamamatsu Photonics K.K. *Handboook:SI apd and mppc*.

[34] S. Cova. "Avalanche photodiodes and quenching circuits for single-photon detection". In: *Applied Optics* ().

[35] A.Blondel. "The SuperFGD Prototype Charged Particle Beam Tests". In: (2020). DOI: 10.1088/1748-0221/15/12/P12003. arXiv: 2008.08861.

[36] A. Blondel et al. "The SuperFGD Prototype charged particle beam tests". In: *Nuclear Instruments and Methods in Physics Research Section A: Accelerators, Spectrometers, Detectors and Associated Equipment* 948 (2019).

[37] R.Tamura. "Construction and performance of a neutrino detector for neutrino-nucleus inter- action cross-section measurements". MA thesis. University of Tokyo, 2018.

[38] Isamu.Nakamura. "A 64ch readout module for PPD/MPPC/SiPM using EASIROC ASIC". In: *Nuclear Instruments and Methods in Physics Research Section A: Accelerators, Spectrometers, Detectors and Associated Equipment* 787 (2015), pp. 376–379.

[39] Omega. *EASIROC DATASHEET*. 2011.

[40] Nichia Corporation. *SPECIFICATIONS FOR BLUE LED*. 2020.

[41] A.Nagaia. "Characterization of a large area silicon photomultiplier". In: *Journal of Instru-mentation* 15 (2020).

[42] Shih Kai Liu. *First look at MPPC64-PCB cross check measurements*. 2021.